Published in final edited form as:

Hippocampus. 2016 September ; 26(9): 1189–1212. doi:10.1002/hipo.22603.

SUBCORTICAL CONNECTIONS OF THE PERIRHINAL, POSTRHINAL, AND ENTORHINAL CORTICES OF THE RAT. I. AFFERENTS

Inês Tomás Pereira[1], **Kara L. Agster**[2,*], and **Rebecca D. Burwell**[1,2]

[1]Department of Cognitive, Linguistic, and Psychological Sciences, Brown University, Providence RI, 02912

[2]Department of Neuroscience, Brown University, Providence RI, 02912

Abstract

In this study we characterized the subcortical afferents for the rat PER areas 35 and 36, POR, and the lateral and medial entorhinal areas (LEA and MEA). We analyzed 33 retrograde tract-tracing experiments distributed across the five regions. For each experiment, we estimated the total numbers, percentages, and densities of labeled cells in 36 subcortical structures and nuclei distributed across septum, basal ganglia, claustrum, amygdala, olfactory structures, thalamus, and hypothalamus. We found that the complement of subcortical inputs differs across the five regions, especially the PER and POR. The PER receives input from the reuniens, suprageniculate, and medial geniculate thalamic nuclei as well as the amygdala. Overall, the subcortical inputs to the PER are consistent with a role in perception, multimodal processing, and the formation of associations that include the motivational significance of individual items and objects. Subcortical inputs to the POR were dominated by the dorsal thalamus, particularly the lateral posterior nucleus, a region implicated in visuospatial attention. The complement of subcortical inputs to the POR is consistent with a role in representing and monitoring the local spatial context. We also report that, in addition to the PER, the LEA and the medial band of the MEA also receive strong amygdala input. In contrast, subcortical input to the POR and the MEA lateral band includes much less amygdala input and is dominated by dorsal thalamic nuclei, particularly nuclei involved in spatial information processing. Like the cortical inputs, the patterns of subcortical inputs to these regions are consistent both with the view that the dorsal hippocampus is important for spatial cognition and the ventral hippocampus is important for affective cognition, and the view that they provide considerable functional integration. We conclude that the patterns of subcortical inputs to the PER, POR, and the entorhinal LEA and MEA provide further evidence for functional differentiation in the medial temporal lobe.

Keywords

parahippocampal; anatomy; connectivity; retrograde; memory

Please direct correspondence and reprint requests to: Rebecca D. Burwell, Ph.D, Address: Department of Cognitive, Linguistic and Psychological Sciences, Brown University, Box 1821, Providence, RI 02912, Phone: (401) 863-9208, Fax: (401) 863-1300, Rebecca_Burwell@Brown.edu.

*KLA is currently located in the Department of Psychiatry at the University of North Carolina, Chapel Hill.

Introduction

The cortical regions that surround the rodent hippocampus include three cytoarchitectonically discrete cortical regions, the perirhinal (PER), the postrhinal (POR), and the entorhinal cortices (EC) (Figure 1A). The PER was further subdivided into areas 35 and 36 (Brodmann, 1909; Burwell, 2001; Krieg, 1946). The entorhinal cortex was subdivided into lateral and medial entorhinal areas (LEA and MEA) (Blackstad, 1956; Brodmann, 1909). The parahippocampal region comprises the PER, POR, and EC, along with the presubiculum and parasubiculum. Together, these regions serve as the gateway for unimodal and polymodal associational input directed to the hippocampal formation. Available evidence suggests that these regions process information differently *en route* to the hippocampus and that they may have unique, non-mnemonic functions. Importantly, the PER, POR, and EC show good homology across mice, rats, monkeys, and humans (Amaral et al., 1987; Beaudin et al., 2013; Brodmann, 1909; Burwell et al., 1995; Franko et al., 2014; Insausti et al., 1995; Suzuki and Amaral, 2003). Thus, an understanding of the organization of subcortical connections should provide insight into how information is processed by these regions in the service of memory and other cognitive functions.

We previously investigated the interconnections of the rat PER, POR, and EC (Burwell and Amaral, 1998b), the cortical inputs and outputs (Agster and Burwell, 2009; Burwell and Amaral, 1998a), and connections with the hippocampal formation (Agster and Burwell, 2013). These studies revealed a complex network of projections. To briefly summarize, neocortical input from ventral temporal association cortex as well as unimodal associational input from somatosensory, auditory, and visual areas, targets area 36 of the PER, which then projects to area 35. Interestingly, somatosensory, auditory, and visual areas preferentially target rostral, mid-rostrocaudal, and caudal area 36, respectively (Burwell, 2001). Long-range intrinsic connections likely further integrate information along the rostrocaudal axis of the PER (Unal et al., 2013). The PER also receives substantial input from the LEA, piriform cortex, and insular areas, and these projections preferentially target PER area 35. The POR is heavily innervated by visual association and visuospatial areas, including the retrosplenial and posterior parietal cortices. The cortical efferents are similarly segregated, with POR targeting mainly visual and visuospatial regions and the PER targeting all sensory modalities. The PER is most heavily interconnected with the lateral band of the LEA. The POR is most heavily interconnected with the lateral band of the MEA, but also with caudal LEA (Agster and Burwell, 2013). Interestingly, the POR projects strongly to the caudal PER, which receives the most visual input. All parts of the PER project to the POR, but the strongest input is from the caudal (visual) PER.

The topographies of the PER and POR projections to the LEA and MEA are important because of the organization of the perforant pathway projection to the dentate gyrus of the hippocampal formation. The intrinsic connections of the EC are segregated into three bands organized from the lateral to the medial extent of the cortex (Figure 1B). Each band includes portions of the LEA and the MEA. The bands are organized such that the cells located in a single band are highly interconnected, but project minimally outside the band of origin (Dolorfo and Amaral, 1998a). Each band projects via the perforant pathway to a different

septotemporal component of the hippocampal formation (Dolorfo and Amaral, 1998b). The lateral band projects to the septal half of the dentate gyrus, the intermediate band projects to the third septotemporal quarter, and the medial band projects to the fourth quarter. This connectional topography suggests that the organization of pathways through the PER, POR, EC, and the hippocampal formation supports functional differentiation in the hippocampal system. Thus, it is also important to know the organization of subcortical input to lateral to medial bands of the LEA and the MEA.

Numerous studies have addressed the subcortical connections of the EC (e.g. Alonso and Kohler, 1984; Beckstead, 1978; Eid et al., 1996; Wouterlood, 1991). Some studies have characterized the PER connections with the amygdala, thalamus, and hypothalamus (Kemppainen et al., 2002; Moga et al., 1995; Pikkarainen and Pitkänen, 2001; van Groen et al., 1999; Vertes et al., 1995). We also previously reviewed the subcortical connections of these regions in summary form (Furtak et al., 2007; Kerr et al., 2007). There are, however, no detailed studies of the subcortical connections of the POR and no studies that permit comparison of subcortical connections across the PER, POR, and EC.

Here, we investigated the origins of subcortical input to the rat PER areas 35 and 36, POR, and the lateral and medial subdivisions of the EC (LEA and MEA). We placed injections of retrograde tracers at distributed locations in each region. For each tract tracing experiment, the total numbers of labeled cells (and cell densities) were estimated for 36 subcortical structures, providing a comprehensive and quantitative assessment of the subcortical inputs to PER areas 36 and 35, POR, LEA, and MEA. A parallel study used anterograde tract tracers to assess the subcortical efferents of these regions (Agster et al., submitted). Taken together, the two studies allow for comparison of the subcortical afferents and efferents across subcortical structures and across the target parahippocampal structures.

Materials and Methods

Nomenclature

Target regions—For the PER areas 35 and 36 and the POR, we used boundaries and histological criteria proposed by Burwell (2001). In some nomenclatures, PER area 35 is called perirhinal cortex and PER area 36 is called ectorhinal cortex (Paxinos and Watson, 1998; Swanson, 1998). Those sources do not include the POR, but the combined perirhinal and ectorhinal cortices caudal to the angular bundle are roughly comparable. For the EC, we used the parcellation into LEA and MEA proposed by Brodmann (1909), Lorente de No (1933), and Blackstad (1956). The entorhinal cortex has been further subdivided into six subareas (Insausti et al., 1997), but for the purposes of this report we will use the LEA/MEA parcellation. The borders and nomenclature for the subcortical regions in which we quantified numbers of labeled cells are adapted from the atlases of Swanson (1992) and Swanson (1998). The subcortical structures are enumerated in Table 1 along with the abbreviations used in all figures and the text. A subset of coronal sections illustrating those structures is shown in Figure 2. In order to have a manageable number of structures for quantification, in some cases it was necessary to combine nuclei and subnuclei.

Olfactory regions—Following Swanson (1992), the olfactory areas analyzed were the anterior olfactory nucleus (AON), the olfactory tubercle (OT), the piriform transition area (PTA), the endopiriform nucleus (EP), and the taenia tecta (TT, Table 1). The AON included all layers of the dorsal and external parts of the anterior olfactory nucleus. The OT included all three layers plus the islands of Calleja. The PTA included the postpiriform transition area and the piriform-amygdaloid area. The EP included the dorsal and ventral subnuclei. We included the taenia tecta in the olfactory areas as has been previously done on connectional and cytoarchitectonic grounds (Gurdjian, 1925; Haberly and Price, 1978).

Claustrum—The claustrum (CLA) is implicated in numerous functions, although the most enduring proposal is that the region subserves sensorimotor integration. It has widespread connections with neocortical and subcortical structures (Witter et al., 1988). For those reasons, we refrained from grouping the region with other subcortical structures and have analyzed its connections individually.

Amygdala—The amygdala complex was grouped into five regions — the lateral nucleus (LA), the basolateral nucleus (BLA), the basomedial nucleus (BMA), the central nucleus (CEA), and the olfactory amygdala (OA). We followed Swanson (1992) and Krettek and Price (1978) for most of these groupings. The LA, BLA, and CEA were analyzed as individual structures. The BMA region was a composite of the basomedial nucleus, the posterior nucleus, and the intercalated nuclei of the amygdala. We included the latter two nuclei with the BMA because they appear to belong to the deep nuclei of the amygdala and are in closest proximity with the BMA (Canteras et al., 1992). The OA included the structures that receive direct input from the olfactory bulb or the accessory olfactory bulb, including the nucleus of the lateral olfactory tract, the bed nucleus of the accessory olfactory tract, the anterior amygdaloid area, the medial nucleus, and the cortical nucleus (de Olmos et al., 1978; Gurdjian, 1925).

Septal nuclei—For the septal afferents, we analyzed four regions, including the lateral septal nucleus (LS), the medial septal complex (MS), the posterior septal complex (PS), and the bed nucleus of the stria terminalis (BST). Following Swanson (1992), the LS comprised the dorsal, intermediate, and ventral parts. The MS comprised the medial septal nucleus and the nucleus of the diagonal band. The PS included the septofimbrial nucleus and the triangular nucleus of the septum. The BST included all of the areas and nuclei in the anterior and posterior divisions as well as the septohippocampal nucleus and the subfornical organ.

Basal ganglia—We grouped structures in the corpus striatum with midbrain structures on functional grounds. In the corpus striatum, we analyzed the caudate putamen (CP), the nucleus accumbens and the fundus of the striatum (ACB), the lateral and medial segments of the globus pallidus (GP), and the substantia innominata including the magnocellular preoptic nucleus (SI) (Swanson, 1992). We included the dopaminergic cell groups in the substantia nigra pars compacta and pars reticulata with the ventral tegmental area (SN-VTA).

Dorsal thalamus—In general, we used Swanson (1992) and Jones (1985) in the delineation of borders for the quantitative analyses. The epithalamus (EPI) included the lateral and medial habenula. For the dorsal thalamus, except for the geniculate regions, we

used Swanson's groupings. We quantified labeled cells in the midline group (DTHmi), the anterior group (DTHan), the medial group (DTHme), the lateral group (DTHla), and the ventral group (DTHve). DTHmi included the paraventricular nucleus, the parataenial nucleus, and the nucleus reuniens. DTHan included the anteroventral, anteromedial, anterodorsal, interanteromedial, interanterodorsal, and lateral dorsal nuclei of the thalamus. DTHme included the mediodorsal and submedial thalamic nuclei and the perireuniens nucleus. DTHla included the suprageniculate nucleus and the lateral posterior nucleus, the posterior limiting nucleus, and the posterior complex of the thalamus. The DTHve included the ventral anterior-lateral complex, the ventral medial nucleus and the ventral posterior complex of the dorsal thalamus. Finally, the intralaminar nucleus of the dorsal thalamus (ILM) was analyzed as a single structure.

Ventrolateral thalamus—The geniculate regions were divided into the medial geniculate complex (MG), which is part of the dorsal geniculate group, and the lateral geniculate complex (LG). LG included the dorsal and ventral parts of the lateral geniculate complex and the intergeniculate leaflet. Ventrolateral thalamic structures quantified included the reticular nucleus (RT) and the zona incerta (ZI). We grouped the remaining ventrolateral thalamic structures (VLTH). The VLTH included the subthalamic nucleus, the perifascicular nucleus, and the peripeduncular nucleus.

Hypothalamus—We analyzed the periventricular zone (PVZ), the medial zone excluding the mammillary body (MEZ), the collected structures of the mammillary body (MBO), and the lateral zone (LZ) following Swanson (1992). The PVZ included the paraventricular nucleus of the hypothalamus as well as the anteroventral, anterior, intermediate, and posterior paraventricular nuclei of the hypothalamus. Also included were the vascular organ of the lamina terminalis, the suprachiasmatic and median preoptic nuclei, the preoptic paraventricular nucleus, and the arcuate nucleus of the hypothalamus. The MBO included the dorsal, medial, and lateral mammillary nuclei, the tuberomammillary nucleus, and the supramammillary nucleus. The MBO is part of the medial zone of the hypothalamus, but we parceled it out for analysis because of its putative role in memory. The remaining medial structures formed the MEZ and included the medial, anterodorsal, anteroventral, and posterodorsal preoptic nuclei, the parastrial nucleus, the suprachismatic nucleus, the retrochiasmatic area, the subparaventriclar zone, the anterior hypothalamic area, and the tuberal area of the hypothalamus. The LZ included the lateral preoptic area and the lateral hypothalamic area.

Subjects

Subjects were 22, previously untreated, male adult Sprague-Dawley rats (Harlan Laboratories, Houston, TX or Charles Rivers Laboratories) weighing between 300 and 400 g. Subjects were housed individually or in pairs under standard 12h light/12h dark conditions with *ad libitum* access to food and water. Following surgery, subjects were housed individually. All methods involving the use of live animals conformed to NIH guidelines and were approved by the appropriate animal care and used committees at Salk Institute for Biological Studies, the State University of New York at Stony Brook, and the Brown University Institutional Animal Care and Use Committees. Data from these subjects

were used in analyses of the cortical afferents, hippocampal connections, and interconnections of the PER, POR, and EC (Agster and Burwell, 2013; Burwell and Amaral, 1998a; Burwell and Amaral, 1998b).

Surgery

Surgical procedures were as previously reported (Burwell and Amaral, 1998a). Briefly, subjects were anesthetized by one of two methods, either intraperitoneal injection of sodium pentobarbital (Nembutal®, Abbott Laboratories, North Chicago, IL, 50 mg/kg) or with halothane gas. Subjects were secured in a Kopf stereotaxic apparatus (Tujunga, CA) in the flat skull position, a craniotomy was drilled above the intended injection site, and a small incision was made in the dura for pressure injection of retrograde dyes via micropipette. The retrograde tracers used (Dr. Illing GmbH and Co., Gross Umstadt, Germany) were either Fast Blue (FB, 150 nL, 3% in distilled H_2O) or Diamidino Yellow (DY, 200 nL, 2% in distilled H_2O). One subject, 108FG, received a single injection of 100 nL of a 2% solution of Fluoro-Gold (FG, Fluorochrome, Inc., Englewood, CO) in 0,9% NaCl (Schmued and Fallon, 1986). Injections were made in the target regions (PER, POR, or EC) using stereotaxic coordinates (Paxinos and Watson, 1986). The tracers were pressure injected through glass micropipettes pulled from capillary tubing (Corning, Inc. Corning, NY) with outer diameter of 800 μm and inner diameter of 250 μm. Micropipette tip diameter was 60–90 μm. The tracers were pressure injected at the rate of 30 nL/min. The micropipette was raised 100 μm immediately following the injection. After a 10 min stabilization period, it was slowly raised at a rate of 500 μm/min until totally removed, as previously described (Burwell and Amaral, 1998b). After one or two injections were completed, the wound was sutured. Subjects were kept warm and under observation for 1–2 hours or until awake, and then were transferred back to the animal colony for a 7–9 day survival period.

Tissue processing

Subjects were deeply anesthetized with a 35% solution of chloral hydrate and transcardially perfused using a pH-shift protocol (Burwell and Amaral, 1998a). Solutions were perfused at a flow rate of 35–40 ml/min. A two min perfusion of room temperature saline was followed by 10 min of 4% paraformaldehyde in 0.1 M sodium acetate buffer (pH 6.5 at 4°C) and 15 min of 4% paraformaldehyde in 0.1 M sodium borate buffer (pH 9.5 at 4°C). Ice was packed around the subject's head after the saline step to cool the brain during perfusion. Brains were removed from the skull, postfixed for 6 h in the second paraformaldehyde solution at 4°C, and cryoprotected for 24 h in 20% glycerol in 0.02 M potassium phosphate buffered saline (KPBS, pH 7.4 at 4°C). The brains were then frozen, and immediately sectioned or stored at −70°C.

The brain was cut into five series of 30 μm sections beginning at the rostral limit of prefrontal cortex and extending through the caudal pole of the neocortex. One 1:5 series was collected into 0.1 M phosphate buffer (PB), and later mounted and stained for Nissl material. A second series was also collected into 0.1 M PB, and immediately used for retrograde tracer procedures explained below. The remaining three series were used for other procedures or stored at −70°C in cryoprotectant solution (Burwell and Amaral, 1998b).

Sections analyzed for fluorescent retrogradely-labeled cells were mounted onto gelatin-coated slides after sectioning. The mounted tissue was dried at room temperature for 2–4 h in a vacuum desiccator, dehydrated in 100% ethanol (2 × 2 min), cleared in xylene (3 × 2 min), and coverslipped with DPX Mountant (Gallard-Schlessinger, Plainview, NY). This technique improves visibility and prevents fading of fluorescent dyes indefinitely, with moderate increases in background fluorescence.

Data analysis

Thirty-three labeled cells tracer injections in the PER, POR and EC were selected for analysis from a library of 72 cases (Table 2). These cases were previously used to describe the cortical, hippocampal, and parahippocampal connections of the PER, POR and EC (Agster and Burwell, 2013; Burwell and Amaral, 1998a; Burwell and Amaral, 1998b).

Regional borders for the subcortical areas designated in Table 1 were determined based on Swanson (1992) and Swanson (1998). See detailed discussion under Nomenclature. Contours were drawn and fluorescently labeled cells were plotted for a 1:10 series of 30 μm sections throughout the selected subcortical regions ipsilateral to the injection site. A range of 42 to 48 coronal sections were quantified for each experiment. Labeled cells were plotted at a total magnification of 100× (10× objective X 10× eyepiece) using a Nikon Optiphot-2 or a Nikon E600 coupled to a computerized data collection system (Neurolucida, MicroBrightfield, Inc., Burlington, VT). For each section, the area of each contour and the total number of cells within the contour were quantified by Neurolucida and exported to Excel. Total cell counts within the area contours were quantified for every section in the 1:10 series. Stereological methods were not used. Total numbers of labeled cells were estimated by multiplying the number of cells plotted in the 1:10 series by 10. Cell numbers were then normalized to the mean total number of cells labeled in cortical, subcortical, and hippocampus regions for all injection sites. The estimated volume of each afferent region was estimated by summing the areas of the contours and multiplying by the 300-μm step size between sections along the z-axis. It is possible these estimates could be biased by increased probability of double counting along the z-axis as well as by loss of caps due to the difficulty in identifying partial cell bodies at the margin of a coronal section. These biases are not likely to significantly impact the interpretation of results for two reasons: first, the two types of biases are in opposite directions; and second, the estimates of cell number and density in all subcortical regions were subject to the same bias.

Primary analysis provided estimated total numbers of cells labeled in each region for each case. We further analyzed these data by two complementary methods. These secondary analyses comprised the density of labeled cells in the subcortical afferent regions, and the percentage of total input to the target regions. Densities of labeled cells were calculated as the total normalized number of cells in each region divided by the volume of the region. We also calculated the percent of input arising from the afferent regions to a particular target structure. The percentages were based on the total numbers of labeled cells observed in each subcortical afferent region.

The density and percentage measures provide qualitatively different views of the impact of subcortical afferents to the PER, POR, and EC. The density of labeled cells allows assessing

whether a particular subcortical region projects more strongly to one target region than another. The percentage measure is more useful for understanding the pattern of inputs to a particular target region. In other words, does a particular target region receive more input from one subcortical structure than another. The percentage measure also allows comparison of the overall pattern of subcortical input across target regions. Thus, both measures can be used the assess pattern and strength of projections. The density measure is more useful for assessing the strength and pattern of output from subcortical afferent regions, whereas the percentage measure is more useful for examining the relative strength and pattern of input to target regions. The contribution and use of these two measures is elaborated in the discussion.

Finally, we used correlation analysis to quantify the similarities of subcortical afferentation of the target regions. A pairwise Pearson correlation analysis of the percentage measure was performed across all pairs of the five parahippocampal target structures. We chose the percentage measure because that measure represents the patterns of subcortical afferentation and is not biased by either the volume of subcortical afferent regions or the overall size of the projection. Statistical significance was set at $p < 0.05$.

Results

Description of injection sites

Thirty-three injections of labeled cells dyes were made in various locations of the PER, POR and EC (Figure 1C and Table 2). The area of the injection site was defined as the dye core plus the region of heavy necrosis immediately surrounding the dye core. Figure 2 shows color-coded boundaries of the quantified regions on coronal views (see abbreviations in Table 1). Figures 3 through 7 show the injection site and labeled cells in nine coronal sections for representative labeled cells dye injections located in areas 35, 36, POR, LEA and MEA. Although injection size varied, as previously reported (Burwell and Amaral, 1998a), there were no significant differences among the five target regions in mean volume of the injection sites ($p > 0.43$). Figure 8 shows a summary of the analysis for the composite subcortical areas, to facilitate comparison between regions.

Percentage of subcortical input

Table 3 shows the percentage of total input to the parahippocampal target regions arising from each subcortical region. The normalized mean total number of subcortical cells labeled for each target region is shown at the bottom of Table 3. Thus, the mean number of cells labeled in each subcortical region can be calculated from the table.

Perirhinal cortex area 35—The PER area 35 shows strong subcortical connectivity as judged by total normalized labeled cells of 69,400 (Table 3 bottom, and Figure 8B). Based on percentages of labeled cells, the principal subcortical afferents to area 35 originate in the olfactory regions, accounting for one third of all subcortical inputs (33%). This is followed closely by the claustrum (21%), the amygdala (20%), and the thalamus (20%, Table 3, Figure 8A). Most of the olfactory input arises from the EP (20%) and PTA (11%),

subcortical structures associated with piriform regions (Figure 3F,G). Both the EP and the PTA project to all rostro-caudal levels of area 35.

All subdivisions of the amygdala project to area 35, and all regions, particularly the LA project preferentially to caudal area 35. The input from LA, BLA, and BMA, account for approximately 7%, 4%, and 5% respectively. Consistent with the olfactory inputs, the OA also provides 5% of the total subcortical input to area 35.

The claustrum (Figure 3D, E) projects strongly to all rostro-caudal regions. Area 35 receives moderate projections from the dorsal thalamus that mainly arise from DTHmi, DTHla (Figure 3G), and the ILM. The projection from DTHmi originates primarily from the nucleus reuniens, and the input from DTHla is observed from all nuclei in this subdivision except for the lateral posterior nucleus. The MG, or the auditory thalamus, provides a strong input that targets the mid-rostrocaudal portion of area 35 (Figure 1C, case 112DY, and Figure 3H). The remaining nuclei of the ventrolateral thalamus along with the septal nuclei, the basal ganglia, and the hypothalamus provide few afferents to area 35 (Table 3).

Perirhinal cortex area 36—For PER area 36 labeled cells transport resulted in approximately 47,900 labeled cells, more than the POR, but less than the other areas (Table 3 bottom, and Figure 8B). Based on percentages of labeled cells, inputs to area 36 are dominated by the amygdala and the thalamus (approximately 40% each, Table 3, Figure 8A). Of the amygdala inputs, the LA contributes most heavily and these projections terminate in the mid-rostrocaudal and caudal portions of area 36. The representative case shown in Figure 4F, 98DY, provides a good example as the injection site is located in mid-rostrocaudal area 36 (Figure 1C).

Similarly to the amygdala, the thalamic nuclei contribute strong afferent projections to area 36 (Table 3). The largest projection from the dorsal thalamus to area 36 originates in DTHla (16%, Figure 4G) and terminates more strongly in the mid-rostrocaudal level. This projection arises most strongly from the suprageniculate nucleus. The next strongest projection arises in the MG (Figure 4H) and targets both the rostral and mid-rostrocaudal parts of area 36. The VLTH provides a significant, but more modest input, but cells were observed only in the perifascicular nucleus, and the peripeduncular nucleus (no cells were found in the subthalamic nuclei). Finally, the claustrum and olfactory areas, particularly the PTA, contribute moderate input to area 36. Little or no input to area 36 arises in the septal nuclei, the basal ganglia or the hypothalamus (Table 3).

Postrhinal cortex—The POR receives a smaller complement of subcortical input, judging by the number of labeled cells, 25,500, approximately half or less than that of the other regions (Table 3 bottom, and Figure 8B). This input is dominated by projections from the dorsal thalamus (64%, Figure 8A), with the DTHla representing a striking proportion of the total subcortical innervation (35%, Figure 5F, G). The labeled cells in the DTHla were confined entirely to one thalamic nucleus, the lateral posterior nucleus. The strongest labeling resulted from injection sites located more caudally in the POR. This projection accounts for approximately half of the input from dorsal thalamus to the POR. Although the thalamic input is dominated by the lateral posterior nucleus, the DTHan, ILM and DTHmi

also provide strong afferent innervation to the POR. Input from DTHan was primarily localized to the anterodorsal, anteromedial and lateral dorsal nuclei, the ILM projection originated particularly from the rhomboid nucleus, and in the DTHmi most labeled cells were found in the nucleus reuniens.

The second largest subcortical input to the POR after the lateral posterior nucleus arises in the claustrum (Figure 5B, C). This projection accounts for approximately one-fifth of the total subcortical input in percentages of labeled cells (Table 3). These projections terminate preferentially in the rostral and mid-rostrocaudal levels of the POR.

More modest numbers of labeled cells were observed in the ventrolateral thalamus, hypothalamus, amygdala and septal regions. The majority of ventrolateral thalamus input to POR is provided by the ZI and VLTH. Input from the hypothalamus originated primarily in MBO and LZ (Table 3). From the amygdala, the LA and BLA provide the strongest inputs, though this input is weak compared to PER afferents. The modest input from the septal region arises almost entirely from the MS, and inspection of the individual cases indicates that this projection arises in the diagonal band of Broca. Finally, the olfactory regions and the basal ganglia provide minimal input to the POR.

Lateral entorhinal area—Retrograde tract tracer injections into the LEA resulted in a normalized total of approximately 89,800 labeled cells (Table 3 bottom, and Figure 8B). The highest proportion of labeled cells originated in olfactory areas, accounting for more than one-third of the total input from subcortical regions (Table 3, and Figure 8A). Within the olfactory region, afferents arise predominately from EP and PTA (Table 3, Figure 6E–H). These areas project more strongly to the intermediate and medial bands, but the lateral band is also strongly targeted. The LEA also receives a large percentage of input from the claustrum (20%, Figure 6C, D), with little bias for each of the cortical bands, and the amygdala (25%), particularly to the intermediate and medial bands. From the amygdala, OA, LA and BMA contribute the most input to the LEA (Figure 6E, F). Afferents from the dorsal thalamus (12%), particularly DTHmi (9%), also contribute to the input to all bands of the LEA (Table 3). Labeled cells were observed in all subregions of the DTHmi, but densities were higher in the nucleus reuniens. Other smaller but noteworthy projections arrive to the LEA from the septal nuclei (mainly MS), and the hypothalamus (mainly MBO). Afferents arising from the basal ganglia and ventrolateral thalamic nuclei provide minimal input to the LEA.

Medial entorhinal area—The MEA receives strong subcortical input, roughly comparable to that of area 35, with 63,800 cells (Table 3 bottom, and Figure 8B). Injections in the MEA resulted in strong labeling in the olfactory nuclei (23%), the amygdala (27%), and the dorsal thalamus (22%, Table 3, Fig 8A). Olfactory input is dominated by EP projections terminating mainly in the intermediate and medial bands of the MEA (Figure 7F). From the amygdala nuclei, OA accounts for the largest percentage of labeled cells (Table 3, Figure 7F). These projections terminate mostly in the medial band of the MEA. From the dorsal thalamus, the vast majority of labeled cells was observed in DTHmi, more specifically in the nucleus reuniens (Figure 7D) and particularly targeted the medial band. The claustrum also provides strong input to the MEA (17%, Figure 7D) and this projection

is fairly uniform across MEA bands. MEA injections also result in labeled cells in the hypothalamus, especially if the injection is in the lateral band of MEA. The main contributors to the hypothalamic input to the MEA are MBO and LZ (Table 3). The septal nuclei contribute a relatively small percent of total subcortical input, with the majority of this input originating in MS. The MEA also receives a small percent of input from the basal ganglia and ventrolateral thalamus.

Similarity of projections across parahippocampal structures—To compare the similarity of projections among the five parahippocampal structures, a pairwise Pearson correlation analysis was performed using the percentage measure from Table 3. The pattern of inputs to LEA, MEA and PER area 35 were highly intercorrelated with Pearson r-values ranging from 0.842–0.943 ($p < 0.001$). In contrast, the intercorrelations among the POR, PER area 35 and PER area 36 were weaker, though still significant, with Pearson r-values ranging from 0.350 to 0.415 ($p < 0.036$). Finally, the comparisons of input pattern between POR and EC (both LEA and MEA), and between PER area 36 and EC (LEA and MEA) did not show statistically significant correlations.

Average density of labeled cells

Table 4 shows the average density of labeling, that is, the total normalized number of cells in each region divided by the volume of the region. This measure allows for comparisons of the strength of the projection from one specific subcortical nucleus to the different target regions.

Olfactory areas—Analysis of the density of labeled cells indicates that the subcortical olfactory nuclei project more strongly to the LEA and PER area 35 than to the other area of PER, POR and MEA (Table 4, and Figure 8C). The specific nuclei that project to both LEA and area 35 are also similar, with the PTA and EP showing the strongest density for both regions (Figure 3F, G and Figure 6E–H). Injections of labeled cells tracer in the MEA also leads high density of cells in the EP. The POR and PER area 36 receive relatively weak projections from the olfactory nuclei.

Claustrum—The claustrum shows high density of labeled cells following injections in all target regions (Table 4 and Figure 8C, blue bars). The strongest projections target area 35, LEA and MEA (Figure 3D, E; Figure 6C, D; Figure 7D).

Amygdala—The amygdala projects strongly to PER areas 35 and 36 and both the LEA and MEA (Table 4 and Figure 8C, green bars). The projection from the LA to area 36 is responsible for the highest density of labeling observed in this study (Figure 4F). The LA and the BLA project more strongly to areas 35 and 36, whereas the BMA and OA project more strongly to LEA and MEA (Figure 6E and Figure 7F).

Septal nuclei—The density of cells in the septal nuclei following injections of labeled cells tracer in the target regions was, in general, modest (Table 4 and Figure 8C). For injection sites in each region, the strongest contributor of projections is the MS. This region

sends moderately strong projections to LEA and MEA, intermediate projections to PER area 35 and POR, and weaker projections to PER area 36.

Although the septal input is relatively modest when assessed in the framework of the entire complement of subcortical inputs, these inputs are functionally important for reasons that are described elsewhere. Although we did not address cholinergic and noncholinergic origin of these inputs, these data are available. Briefly, the proportion of basal forebrain projection cells that are cholinergic is higher for the perirhinal and postrhinal cortices (26–48%) than for the entorhinal cortex (13–30%) (Kondo and Zaborszky, 2016).

Basal ganglia—The basal ganglia, overall, show low density of cell labeling following injections of labeled cells tracers into all regions analyzed here (Table 4 and Figure 8C). Among these modest projections, the strongest are observed from CP and SN-VTA to PER area 36, and from SI to PER area 35 (Table 4).

Dorsal thalamus—The dorsal thalamus, taken as a whole, seems to evenly target all five parahippocampal structures (Figure 8C). Further analysis of the subnuclei, however, shows very specific patterns of projections (Table 4). The DTHla, in particular, shows high density of cells following injections to PER area 35, PER area 36, and to POR, but their origin is different. The lateral posterior nucleus strongly projects to POR, but does not project to either PER region (Figure 3G, Figure 4G and Figure 5F, G). The DTHmi, on the other hand, projects to all regions, but more strongly to LEA and MEA, consistent with earlier reports (Berendse and Groenewegen, 1991). These projections originate mainly in the nucleus reuniens for all targets (see, for example, Figure 7D). Other projections of note from the dorsal thalamus include a strong projection from DTHan to MEA, and a strong projection from ILM to POR.

Ventrolateral thalamus—The ventrolateral thalamus, with a few exceptions shows weak connectivity with the five parahippocampal structures (Table 4 and Figure 8C). Those exceptions are notable for the high density of cells observed. The MG (the auditory thalamus) projects strongly to both PER area 35 and PER area 36 (Figure 3H and Figure 4H). Additionally, the VLTH projects to both PER areas, but more strongly to area 36.

Hypothalamus—Overall, the hypothalamic projections to the target regions are weak (Table 4 and Figure 8C). The projection from MBO to both LEA and MEA is the strongest observed, but nonetheless in the intermediate range when compared to the overall analysis.

Dentate gyrus-projecting bands of the entorhinal cortex

For the LEA, there were three injections in the lateral band, four in the intermediate band, and only one in the medial band. For the MEA, there were three injections in the lateral band, two in the intermediate band, and again only one in the medial band. The injections in the LEA and MEA medial bands primarily included deep layers. Although there were different numbers of injection sites in each band, taken together the cases represented input from both deep and superficial layers.

All three bands in LEA received substantial input from the claustrum with injections in all bands resulting in high densities of labeled cells (blue bars in Figure 9B, top). The percent input arising from amygdala nuclei (green sections in Figure 9A, top) and densities of labeled cells in those nuclei (green bars in Figure 9B, top) increased from the lateral to intermediate to medial bands of the LEA. The increase was observed for all amygdala structures that project strongly to the LEA, i.e. all structures except the CEA. The olfactory input also shows a tendency to increase along the lateral to medial bands of the LEA (orange bars in Figure 9B, top), especially for the EP. The projections from dorsal thalamic structures are roughly equally strong across bands (violet bars in Figure 9B, top).

For the MEA, we have noted that there are overall fewer labeled cells arising from subcortical regions. This is especially the case for the lateral MEA in which only the claustrum shows high densities of labeled cells (Figure 9B, bottom). All three MEA bands receive strong input from the claustrum (blue bars in Figure 9B, bottom), though not as strong as the LEA (blue bars in Figure 9B, top). Like the LEA, the percent input arising from amygdala nuclei (green sections in Figure 9A, bottom) and densities of labeled cells in those nuclei (green bars in Figure 9B, bottom) increased from the lateral to intermediate to medial bands of the MEA. With the exception of the MEA lateral band, the densities of labeled cells are similar for the LEA and MEA bands. Again, the increase was observed for all amygdala structures except the CEA. The olfactory input also shows a tendency to increase along the lateral to medial bands of the MEA (orange bars, Figure 9B, bottom). Like the LEA, this increase is especially notable for the EP. All three bands receive input from the dorsal thalamus (violet bars in Figure 9B, bottom) and the input to the intermediate and medial MEA bands is stronger than that to the LEA.

Discussion

We examined the subcortical afferents to the PER, POR, and EC using quantitative labeled cells tract tracing methods. Prior studies have described specific point-to-point connections of individual subcortical regions for one or more of the five target areas, but many of the projections described in this and the accompanying study (Agster et al., submitted), particularly those pertaining to the POR, have not been previously described. Moreover, our quantitative, multi-target approach facilitates comparison of strength and patterns of subcortical projections across the target regions.

Our data analysis procedures quantified subcortical afferents in two ways, providing different insights into our findings. The percentage measure was based on numbers of labeled cells, regardless of the volume of the afferent region. Thus, the percentage measure is suitable for assessing the pattern of input to a particular target region and for comparing the patterns of input across target regions (Table 3 and Figure 10). The density measure does include the volume of the subcortical region in that the total number of labeled cells in the structure is divided by its volume. This measure is suitable for comparing the size of the output from a single afferent region across target regions (Table 4 and Figure 11).

One asset of our study is that we normalized the data to control for differences that might result from the size of injection sites or the efficacy of transport. Because we plotted labeled

cells throughout cortical, subcortical, and hippocampal regions for each of the cases, we were able to normalize our data on the assumption that injection sites of similar size and efficacy would result in comparable numbers of labeled cells. This approach strengthens the comparison of inputs across different areas in the parahippocampal region. A caveat, of course, is that even an accurate estimate of numbers of labeled cells labeled neurons in a particular subcortical region does not account for differences in the strength of synaptic contacts. These quantitative data, however, do provide important background information that can inform studies of synaptic connectivity for the afferent and target regions analyzed. Another caveat is that our analyses are based on the assumption that the input to the group of injection sites selected for analysis is representative of the complement of subcortical inputs to the entire target region. Although unlikely, we may have missed a subcortical projection with a highly restricted terminal field in one of our target regions. To guard against this occurrence we analyzed a well-distributed set of injection sites in each target region.

Subcortical influence over hippocampal input pathways

According to a prominent view of medial temporal lobe function, neocortical input is functionally organized into two largely separate information streams: the PER and LEA process nonspatial information about objects and individual items, whereas the POR and MEA process information about space and contexts. In addition, the cortical afferents of the PER and LEA are more similar, whereas the cortical afferents of the POR and MEA are more similar (Burwell and Amaral, 1998a). These two information streams are combined in the hippocampus to support associative learning and episodic memory (Burwell, 2000; Eichenbaum, 2000; Zola-Morgan et al., 1991). An interesting question, then, is how subcortical input might influence these information pathways. Our quantification of subcortical inputs allowed us to address this question by conducting pairwise correlational analyses across the five target regions for the percentages of inputs arising from each of the 36 afferent regions. Interestingly the LEA, MEA, and PER area 35 were significantly and highly intercorrelated. These three regions are similar in that they each receive substantial input from olfactory regions and the amygdala, whereas area 36 receives much less olfactory input and the POR receives little olfactory or amygdala input (Figure 8A). Interestingly, in the rat, area 35 projects to entorhinal cortex more strongly than area 36, whereas area 36 largely projects more strongly to most neocortical regions than area 35 (Agster and Burwell, 2009; Burwell and Amaral, 1998b). This finding suggests that subcortical olfactory and amygdala input strongly influence cortical input to the hippocampus via area 35, the LEA, and the MEA.

Consideration of the EC dentate-gyrus projecting bands reveals a somewhat different picture. Subcortical input to the LEA and the MEA is quite different at the level of the lateral band, which projects to the septal half of the hippocampal formation (Figure 9). Injections in the lateral band of the MEA resulted in a pattern of labeling dominated by the dorsal thalamus with much smaller projections arising from olfactory regions and the amygdala. The olfactory input is strong to all bands of the LEA, but only to the intermediate and medial bands of the MEA. The amygdala input is strong to the intermediate band and strongest to the medial band. These bands project to the temporal half of the hippocampus. The pattern of subcortical input to the LEA and MEA could be construed as consistent with

a prominent view that dorsal hippocampus is more involved in spatial memory, and the ventral hippocampus is more involved in emotional memory. However, it could also be argued that the complexity of the subcortical connections combined with the extensive longitudinal connections of the hippocampal formation affords considerable functional integration.

Parahippocampal connectivity with the claustrum

The robust input from the claustrum to the PER, POR, and EC also deserves discussion. Not much is known about the function of the claustrum but its widespread reciprocal connections with sensory and associational regions of neocortex have prompted suggestions that it participates in sensory integration, perceptual binding, attentional modulation, and consciousness (Crick and Koch, 2005; Goll et al., 2015). The claustrum provides a large proportion of input, about 20%, to PER area 35, POR, and the LEA, about 16% to the MEA, and over 7% to PER area 36. Based on densities of labeled cells, the claustral output is very strong to area 35, LEA, and MEA and less strong to PER area 36 and POR. We should note, however, that injections in all five regions resulted in relatively high densities of labeled cells in the claustrum. Similarly in the monkey, the claustrum provides a very strong input to all temporal lobe structures including all parts of the entorhinal cortex (Insausti et al., 1987; Mufson and Mesulam, 1982; Pearson et al., 1982). In the companion paper (Agster et al., submitted) we report that the PER areas 35 and 36 and the LEA project more strongly to the claustrum than do the POR and the MEA. Whereas the function of the claustrum remains unclear, it is in good position to modulate corticocortical connectivity as well as information flow to and from the hippocampal formation.

Subcortical influence over affective functions

The strongest amygdala projection we observed is from the LA to PER area 36, but projections to area 35, LEA, and the MEA medial band are also strong. These projections are largely reciprocated (Agster et al., submitted). Other studies have assessed the connections of the PER, POR, or EC with the amygdala in rat (Amaral and Price, 1984; Deacon et al., 1983; Majak and Pitkanen, 2003; Pikkarainen and Pitkänen, 2001; Pitkänen et al., 2000; Room and Groenewegen, 1986), cat (Room and Groenewegen, 1986), and monkey (Amaral and Price, 1984; Insausti et al., 1987), but our studies are the only ones that assessed the efferents and afferents of all three regions and their subdivisions.

The strong amygdala input to the PER is consistent with the view that the PER not only processes information about items and their features, but it also encodes the motivational significance of cues. For example, damage to the PER impairs learning of associations between cues and reward schedules (Murray and Richmond, 2001). PER neurons signal associative relationships between cues and reward schedules (Liu and Richmond, 2000), and they signal outcomes associated with cues (Eradath et al., 2015). A related line of research shows that PER connections with the amygdala and thalamus are important for associating cues with negative outcomes. As we show here, the MG, also known as the auditory thalamus, provides strong input to the PER. An earlier report described a projection from the suprageniculate nucleus, but not the MG (Kimura et al., 2003). We also know that the PER projects strongly back to the amygdala (Agster et al., submitted). Romanski and LeDoux

(1992) showed that lesions of the thalamo-amygdala or thalamo-perirhinal-amygdala pathways alone did not impair auditory fear conditioning, but combined lesions of both pathways do impair this behavior. One possibility suggested by the authors is that the thalamo-amygdala pathway provides a fast, but crude representation of auditory information to the amygdala, whereas the thalamo-perirhinal-amygdala pathway provides a slower signal but the representation is more elaborate. This finding is consistent with studies showing that the PER is necessary for associating fear with complex, but not simple, auditory stimuli (Kholodar-Smith et al., 2008).

Previous electrophysiological and anatomical studies of the projections from the amygdala to the EC described a strong projection from BLA to EC, particularly to LEA (Finch et al., 1986; Room and Groenewegen, 1986). Our results reveal a more complex composition of amygdala inputs to the EC. The strongest projection to both LEA and MEA originates in OA, followed by LA, BMA and finally BLA. This pattern of connections is similar to that in monkeys in that the EC is targeted by the lateral and basal amygdala as well as olfactory amygdala structures (Insausti et al., 1987; Pitkanen et al., 2002). Interestingly, inhibition of the BLA input to EC during acquisition of contextual fear conditioning, reduced the freezing response in mice (Sparta et al., 2014). Like PER neurons, EC neurons signal associative relationships between cues and reward schedules; however, different information was encoded by the two regions, arguing against a feedforward signal from the PER (Sugase-Miyamoto and Richmond, 2007). Thus, the LEA and PER may represent complementary aspects of the motivational significance of individual cues.

Because the POR is involved in contextual learning and attentional orienting, its connections with the amygdala are also of interest. Prior studies reported that the main amygdala input to the POR arises in the LA, but that this input is relatively weak (Pikkarainen and Pitkänen, 2001; Pitkänen et al., 2000). We also show that the most input arises from the LA, followed by the BLA. Interestingly, the return projections target the LA and the CEA with similar strength (Agster et al., submitted). The POR projection to the CEA may support the POR role in attentional orienting and in monitoring the current context for changes (Bucci and Burwell, 2004; Burwell and Hafeman, 2003).

Subcortical contributions to PER and POR functions

Available evidence suggests that the PER and POR form different categories of conjunctive or hierarchical representations that contribute to memory, but that are also available to regions outside of the medial temporal lobe for cognitive processes other than memory (Ho and Burwell, 2014; Kent et al., 2016; Ranganath and Ritchey, 2012). Conjunctive coding in the PER represents the complexity of individual stimuli, including relative familiarity and motivational significance (Bussey and Saksida, 2005). Conjunctive coding in the POR represents the spatial layout of items and patterns in the local environmental context (Furtak et al., 2012). Both cortical and subcortical connections are consistent with the view that the PER and POR are key components in circuits whose functions go beyond that of merely providing specific types of information to the medial temporal lobe.

Lesions of the PER impair perceptual discrimination, particularly for multi-feature and multimodal stimuli (Eacott et al., 2001; Goulet and Murray, 2001; Moran and Dalrymple-

Alford, 2003; Saksida et al., 2007). The role for the PER in perception seems to be largely independent of the hippocampus and constitutes a central function of the region. Another function involves signaling familiarity and novelty. The PER has been shown repeatedly to be necessary for the recognition of familiar objects (Ennaceur and Aggleton, 1997; Winters and Bussey, 2005) and to have different neural signatures for familiar and novel objects (Wan et al., 1999; Zhu and Brown, 1995). Recently, our laboratory showed that PER stimulation at specific frequencies influences behavioral exploration of familiarity and novelty (Ho et al., 2015), suggesting the PER is part of a circuit that upregulates and downregulates exploratory behavior based on current surroundings and internal states.

The cortical and subcortical input to the PER is consistent with a role in processing detailed and multimodal information about objects and discrete items including behavioral relevance, like relative familiarity. The PER receives multimodal sensory inputs, roughly segregated along the anteroposterior axis (Burwell, 2001; Burwell and Amaral, 1998a). The subcortical input could support this capability to integrate information across modalities. A moderate projection to the entire rostrocaudal extent of area 35 originates in the midline thalamic structures, implicated in attention, and in the nucleus reuniens, implicated in crossmodal processing (Van der Werf et al., 2002). Area 36 receives a strong input from the suprageniculate thalamic nucleus in the DTHla. The suprageniculate nucleus is also implicated in multimodal information processing. These inputs to PER areas 35 and 36 may be important for encoding multimodal, multidimensional stimuli and for disambiguating overlapping features of complex objects.

The POR is interconnected with the retrosplenial cortex, the posterior cingulate, posterior parietal cortex, and visual association cortices (Burwell, 2001; Burwell and Amaral, 1998a). The POR is uniquely situated to process contextual representations, and its subcortical afferents are consistent with this putative function. Two-thirds of the subcortical input to the POR arises in the dorsal thalamus. More than half of that input, however, arises in the lateral posterior nucleus, the rodent homolog of the primate pulvinar nucleus (Kamishina et al., 2009; Nakamura et al., 2015). The rodent lateral posterior nucleus and the primate pulvinar are implicated in visual attention (Posner and Petersen, 1990; Shipp, 2004). Interestingly, the monkey parahippocampal cortex also receives a strong input from the pulvinar (Baleydier and Mauguiere, 1985). The lateral posterior nucleus also targets other cortical regions implicated in visual processes, including the retrosplenial, anterior cingulate, and temporal association cortices (Nakamura et al., 2015). In addition to the lateral posterior nucleus input, POR receives substantial inputs from nucleus reuniens, several anterior nuclei, and the ILM. Of the five target regions, the POR is the only region that receives substantial input from the ILM, an interesting finding, since the ILM has been implicated in attention (Mair et al., 1998; Newman and Burk, 2005).

This pattern of anatomical connections supports functional evidence for a POR role in representing and monitoring spatial context. Based on anatomical and other functional studies (Burwell and Hafeman, 2003; Furtak et al., 2012), we have hypothesized that the POR combines visual and spatial information from the lateral posterior nucleus, visual cortical areas, and the retrosplenial cortex, with object information from PER to represent the spatial layout of items, features, and patterns that characterize a specific context. The

POR is positioned to monitor the current context for changes signaled by the posterior parietal cortex and lateral posterior nucleus, and to update the representation of the current context with identified changes. The POR then makes this contextual information available to a variety of other regions for multiple purposes including decision-making, modulation of behavior, and memory.

Conclusion

This study of the subcortical afferents of PER areas 35 and 36, POR, and the entorhinal LEA and MEA is complemented by the companion study of the subcortical efferents (Agster et al., submitted). These two studies complete a series that includes our prior reports of neocortical and hippocampal afferents and efferents, as well as interconnections among these regions (Agster and Burwell, 2009; Agster and Burwell, 2013; Burwell and Amaral, 1998a; Burwell and Amaral, 1998b). We report that the origin of subcortical input differs among the five target regions providing further evidence for functional differentiation in the medial temporal lobe.

The subcortical inputs to the PER and the POR suggest these areas make different contributions to memory, attention, and other cognitive processes. The PER receives input from multiple sensory modalities from both cortical (Burwell and Amaral, 1998a) and subcortical areas (present study). The PER projects directly to CA1 and subiculum, but it also projects strongly to frontal and other neocortical association regions. Thus, it is in good position to provide information about objects and other discrete stimuli to the hippocampus for memory and to neocortical regions for other cognitive functions. Its sensory input also puts the PER in good position for crossmodal, perceptual, and attentional processing of such stimuli. PER connections with the amygdala likely supports the capability to associate cues with motivational significance. The output of these functions may contribute to decision-making and other cognitive processes through the PER's strong interconnections with frontal associational regions.

The POR is strongly interconnected with retrosplenial and posterior parietal regions, receives visual associational input, and is targeted by the lateral posterior nucleus of the thalamus implicated in visuospatial attention. Like the PER, the POR projects directly to the CA1 and subiculum (Witter et al., 2000). It is also strongly and reciprocally connected with the dorsal presubiculum, also called the postsubiculum (Agster and Burwell, 2013). The dorsal presubiculum is necessary for object location memory and for recognizing familiar environments (Bett et al., 2013). Overall, this pattern of connectivity positions the POR for contextual learning and memory and online representation of the current local context. Such representations are important for episodic memory, but representations of context are also used by other neocortical regions for multiple purposes, for example formation of contextual frames and context-guided behavior.

We conclude that the subcortical inputs to the PER, POR, and EC further differentiate their contributions to hippocampal functions. In addition, the subcortical afferents are consistent with the view that conjunctive coding in the PER represents complex stimuli, including relative familiarity and motivational significance, whereas conjunctive coding in the POR

represents the spatial layout of items and patterns in the local environmental context. Such representations are important for episodic memory, but are also available to regions outside of the medial temporal lobe for non-mnemonic cognitive processes.

Acknowledgments

Grant sponsor: NSF; **Grant number:** IBN9875792 to RDB.

Grant sponsor: NSF; **Grant number:** IOS1146334 to RDB.

Grant sponsor: NIMH; **Grant number:** MH072144 to KLA.

References

Agster KL, Burwell RD. Cortical efferents of the perirhinal, postrhinal, and entorhinal cortices of the rat. Hippocampus. 2009; 19(12):1159–1186. [PubMed: 19360714]

Agster KL, Burwell RD. Hippocampal and subicular efferents and afferents of the perirhinal, postrhinal, and entorhinal cortices of the rat. Behavioural Brain Research. 2013; 254:50–64. [PubMed: 23872326]

Agster KL, Tomás Pereira I, Saddoris MP, Burwell RD. Subcortical connections of the perirhinal, postrhinal, and entorhinal cortices of the rat II Efferents. submitted.

Alonso A, Kohler C. A study of the reciprocal connections between the septum and the entorhinal area using anterograde and retrograde axonal transport methods in the rat brain. The Journal of Comparative Neurology. 1984; 225(3):327–43. [PubMed: 6725648]

Amaral DG, Insausti R, Cowan WM. The entorhinal cortex of the monkey: I. Cytoarchitectonic organization. The Journal of Comparative Neurology. 1987; 264(3):326–355. [PubMed: 2445795]

Amaral DG, Price JL. Amygdalo-cortical projections in the monkey (Macaca fascicularis). The Journal of Comparative Neurology. 1984; 230(4):465–96. [PubMed: 6520247]

Baleydier C, Mauguiere F. Anatomical Evidence for Medial Pulvinar Connections with the Posterior Cingulate Cortex, the Retrosplenial Area, and the Posterior Parahippocampal Gyrus in Monkeys. The Journal of Comparative Neurology. 1985; 232(2):219–228. [PubMed: 3973091]

Beaudin SA, Singh T, Agster KL, Burwell RD. Borders and Comparative Cytoarchitecture of the Perirhinal and Postrhinal Cortices in an F1 Hybrid Mouse. Cerebral Cortex. 2013; 23(2):460–474. [PubMed: 22368084]

Beckstead RM. Afferent connections of the entorhinal area in the rat as demonstrated by retrograde cell-labeling with horseradish peroxidase. Brain Research. 1978; 152(2):249–64. [PubMed: 679029]

Berendse HW, Groenewegen HJ. Restricted Cortical Termination Fields of the Midline and Intralaminar Thalamic Nuclei in the Rat. Neuroscience. 1991; 42(1):73–102. [PubMed: 1713657]

Bett D, Stevenson CH, Shires KL, Smith MT, Martin SJ, Dudchenko PA, Wood ER. The Postsubiculum and Spatial Learning: The Role of Postsubicular Synaptic Activity and Synaptic Plasticity in Hippocampal Place Cell, Object, and Object-Location Memory. The Journal of Neuroscience. 2013; 33(16):6928–6943. [PubMed: 23595751]

Blackstad TW. Commissural connections of the hippocampal region in the rat, with special reference to their mode of termination. The Journal of Comparative Neurology. 1956; 105:417–537. [PubMed: 13385382]

Brodmann, K. Vergleichende lokalisationslehre der grosshirnrinde in ihren prinzipien dargestellt auf grund des zellenbaues. Liepzig: Barth; 1909.

Bucci DJ, Burwell RD. Deficits in attentional orienting following damage to the perirhinal or postrhinal cortices. Behavioral Neuroscience. 2004; 118(5):1117–1122. [PubMed: 15506894]

Burwell RD. The parahippocampal region: corticocortical connectivity. Annals of the New York Academy of Sciences. 2000; 911:25–42. [PubMed: 10911865]

Burwell RD. Borders and cytoarchitecture of the perirhinal and postrhinal cortices in the rat. The Journal of Comparative Neurology. 2001; 437(1):17–41. [PubMed: 11477594]

Burwell RD, Amaral DG. Cortical afferents of the perirhinal, postrhinal, and entorhinal cortices of the rat. The Journal of Comparative Neurology. 1998a; 398(2):179–205. [PubMed: 9700566]

Burwell RD, Amaral DG. Perirhinal and postrhinal cortices of the rat: interconnectivity and connections with the entorhinal cortex. The Journal of Comparative Neurology. 1998b; 391(3): 293–321. [PubMed: 9492202]

Burwell RD, Hafeman DM. Positional firing properties of postrhinal cortex neurons. Neuroscience. 2003; 119(2):577–588. [PubMed: 12770570]

Burwell RD, Witter MP, Amaral DG. Perirhinal and postrhinal cortices of the rat: A review of the neuroanatomical literature and comparison with findings from the monkey brain. Hippocampus. 1995; 5(5):390–408. [PubMed: 8773253]

Bussey TJ, Saksida LM. The perceptual-mnemonic/feature conjunction model of perirhinal cortex function. Quarterly Journal of Experimental Psychology Section B-Comparative and Physiological Psychology. 2005; 58(3–4):269–282.

Canteras NS, Simerly RB, Swanson LW. Connections of the posterior nucleus of the amygdala. The Journal of Comparative Neurology. 1992; 324(2):143–179. [PubMed: 1430327]

Crick FC, Koch C. What is the function of the claustrum? Philosophical Transactions of the Royal Society B-Biological Sciences. 2005; 360(1458):1271–1279.

de Olmos J, Hardy H, Heimer L. The afferent connections of the main and the accessory olfactory bulb formations in the rat: an experimental HRP-study. The Journal of Comparative Neurology. 1978; 181(2):213–244. [PubMed: 690266]

Deacon TW, Eichenbaum H, Rosenberg P, Eckmann KW. Afferent connections of the perirhinal cortex in the rat. The Journal of Comparative Neurology. 1983; 220:168–190. [PubMed: 6643724]

Dolorfo CL, Amaral DG. Entorhinal cortex of the rat: organization of intrinsic connections. The Journal of Comparative Neurology. 1998a; 398(1):49–82. [PubMed: 9703027]

Dolorfo CL, Amaral DG. Entorhinal cortex of the rat: topographic organization of the cells of origin of the perforant path projection to the dentate gyrus. The Journal of Comparative Neurology. 1998b; 398(1):25–48. [PubMed: 9703026]

Eacott MJ, Machin PE, Gaffan EA. Elemental and configural visual discrimination learning following lesions to perirhinal cortex in the rat. Behavioural Brain Research. 2001; 124(1):55–70. [PubMed: 11423166]

Eichenbaum H. A cortical-hippocampal system for declarative memory. Nature Reviews Neuroscience. 2000; 1(1):41–50. [PubMed: 11252767]

Eid T, Jorritsma-Byham B, Schwarcz R, Witter MP. Afferents to the seizure-sensitive neurons in layer III of the medial entorhinal area: a tracing study in the rat. Experimental Brain Research. 1996; 109(2):209–18. [PubMed: 8738371]

Ennaceur A, Aggleton JP. The effects of neurotoxic lesions of the perirhinal cortex combined to fornix transection on object recognition memory in the rat. Behavioural Brain Research. 1997; 88(2): 181–93. [PubMed: 9404627]

Eradath MK, Mogami T, Wang G, Tanaka K. Time context of cue-outcome associations represented by neurons in perirhinal cortex. The Journal of Neuroscience. 2015; 35(10):4350–65. [PubMed: 25762680]

Finch DM, Wong EE, Derian EL, Chen XH, Nowlin-Finch NL, Brothers LA. Neurophysiology of limbic system pathways in the rat: projections from the amygdala to the entorhinal cortex. Brain Research. 1986; 370(2):273–84. [PubMed: 2423179]

Franko E, Insausti AM, Artacho-Perula E, Insausti R, Chavoix C. Identification of the human medial temporal lobe regions on magnetic resonance images. Human Brain Mapping. 2014; 35(1):248–56. [PubMed: 22936605]

Furtak SC, Ahmed OJ, Burwell RD. Single neuron activity and theta modulation in postrhinal cortex during performance on a visual discrimination task. Neuron. 2012; 76(5):976–988. [PubMed: 23217745]

Furtak SC, Wei SM, Agster KL, Burwell RD. Functional neuroanatomy of the parahippocampal region in the rat: the perirhinal and postrhinal cortices. Hippocampus. 2007; 17(9):709–22. [PubMed: 17604355]

Goll Y, Atlan G, Citri A. Attention: the claustrum. Trends in Neurosciences. 2015; 38(8):486–495. [PubMed: 26116988]

Goulet S, Murray EA. Neural substrates of crossmodal association memory in monkeys: The amygdala versus the anterior rhinal cortex. Behavioral Neuroscience. 2001; 115(2):271–284. [PubMed: 11345954]

Gurdjian ES. Olfactory connections in the albino rat, with special reference to the stria medullaris and the anterior commissure. The Journal of Comparative Neurology. 1925; 38(2):127–163.

Haberly LB, Price JL. Association and commissural fiber systems of the olfactory cortex in the rat. I. Systems originating in the piriform cortex and adjacent areas. The Journal of Comparative Neurology. 1978; 178(4):711–740. [PubMed: 632378]

Ho, JW.; Burwell, RD. Space, Time and Memory in the Hippocampal Formation. Vienna: Springer; 2014. Perirhinal and postrhinal functional inputs to the hippocampus; p. 55-81.

Ho JW, Poeta DL, Jacobson TK, Zolnik TA, Neske GT, Connors BW, Burwell RD. Bidirectional Modulation of Recognition Memory. The Journal of Neuroscience. 2015; 35(39):13323–35. [PubMed: 26424881]

Insausti R, Amaral DG, Cowan WM. The entorhinal cortex of the monkey: III. Subcortical afferents. The Journal of Comparative Neurology. 1987; 264(3):396–408. [PubMed: 3680636]

Insausti R, Herrero MT, Witter MP. Entorhinal cortex of the rat: cytoarchitectonic subdivisions and the origin and distribution of cortical efferents. Hippocampus. 1997; 7(2):146–183. [PubMed: 9136047]

Insausti R, Tuñón T, Sobreviela T, Insausti AM, Gonsalo LM. The human entorhinal cortex: A cytoarchitectonic analysis. The Journal of Comparative Neurology. 1995; 355(2):171–198. [PubMed: 7541808]

Jones, EG. The Thalamus. New York: Plenum Press; 1985.

Kamishina H, Conte WL, Patel SS, Tai RJ, Corwin JV, Reep RL. Cortical connections of the rat lateral posterior thalamic nucleus. Brain Research. 2009; 1264:39–56. [PubMed: 19368845]

Kemppainen S, Jolkkonen E, Pitkanen A. Projections from the posterior cortical nucleus of the amygdala to the hippocampal formation and parahippocampal region in rat. Hippocampus. 2002; 12(6):735–55. [PubMed: 12542226]

Kent BA, Hvoslef-Eide M, Saksida LM, Bussey TJ. The representational-hierarchical view of pattern separation: Not just hippocampus, not just space, not just memory? Neurobiology of Learning and Memory. 2016; 129:99–106. [PubMed: 26836403]

Kerr KM, Agster KL, Furtak SC, Burwell RD. Functional neuroanatomy of the parahippocampal region: the lateral and medial entorhinal areas. Hippocampus. 2007; 17(9):697–708. [PubMed: 17607757]

Kholodar-Smith DB, Allen TA, Brown TH. Fear Conditioning to Discontinuous Auditory Cues Requires Perirhinal Cortical Function. Behavioral Neuroscience. 2008; 122(5):1178–1185. [PubMed: 18823174]

Kimura A, Donishi T, Sakoda T, Hazama M, Tamai Y. Auditory thalamic nuclei projections to the temporal cortex in the rat. Neuroscience. 2003; 117(4):1003–1016. [PubMed: 12654352]

Kondo H, Zaborszky L. Topographic organization of the basal forebrain projections to the perirhinal, postrhinal, and entorhinal cortex in rats. J Comp Neurol. 2016 Jan 18. [Epub ahead of print]. doi: 10.1002/cne.23967

Krettek JE, Price JL. A description of the amygdaloid complex in the rat and cat with observations of intra-amygdaloid axonal connections. The Journal of Comparative Neurology. 1978; 178(2):255–280. [PubMed: 627626]

Krieg WJS. Connections of the Cerebral Cortex. 1. The Albino Rat. B. Structure of the Cortical Areas. The Journal of Comparative Neurology. 1946; 84(3):277–323. [PubMed: 20991808]

Liu Z, Richmond BJ. Response differences in monkey TE and perirhinal cortex: stimulus association related to reward schedules. Journal of Neurophysiology. 2000; 83(3):1677–92. [PubMed: 10712488]

Lorente de Nó R. Studies on the structure of the cerebral cortex. I. *Area entorhinalis*. Journal für Psychologie und Neurologie. 1933; 45(2):113–177.

Mair RG, Burk JA, Porter MC. Lesions of the frontal cortex, hippocampus, and intralaminar thalamic nuclei have distinct effects on remembering in rats. Behavioral Neuroscience. 1998; 112(4):772–92. [PubMed: 9733186]

Majak K, Pitkanen A. Projections from the periamygdaloid cortex to the amygdaloid complex, the hippocampal formation, and the parahippocampal region: a PHA-L study in the rat. Hippocampus. 2003; 13(8):922–942. [PubMed: 14750655]

Moga MM, Weis RP, Moore RY. Efferent projections of the paraventricular thalamic nucleus in the rat. The Journal of Comparative Neurology. 1995; 359(2):221–238. [PubMed: 7499526]

Moran JP, Dalrymple-Alford JC. Perirhinal cortex and anterior thalamic lesions: comparative effects on learning and memory. Behavioral Neuroscience. 2003; 117(6):1326–41. [PubMed: 14674851]

Mufson EJ, Mesulam MM. Insula of the Old-World Monkey. 2. Afferent Cortical Input and Comments on the Claustrum. The Journal of Comparative Neurology. 1982; 212(1):23–37. [PubMed: 7174906]

Murray EA, Richmond BJ. Role of perirhinal cortex in object perception, memory, and associations. Current Opinion in Neurobiology. 2001; 11(2):188–93. [PubMed: 11301238]

Nakamura H, Hioki H, Furuta T, Kaneko T. Different cortical projections from three subdivisions of the rat lateral posterior thalamic nucleus: a single-neuron tracing study with viral vectors. The European Journal of Neuroscience. 2015; 41(10):1294–310. [PubMed: 25832313]

Newman LA, Burk JA. Effects of excitotoxic thalamic intralaminar nuclei lesions on attention and working memory. Behavioural Brain Research. 2005; 162(2):264–71. [PubMed: 15970220]

Paxinos, G.; Watson, C. The Rat Brain in Stereotaxic Coordinates. San Diego: Academic Press; 1986.

Paxinos, G.; Watson, C. The Rat Brain in Stereotaxic Coordinates. San Diego: Academic Press; 1998.

Pearson RCA, Brodal P, Gatter KC, Powell TPS. The Organization of the Connections between the Cortex and the Claustrum in the Monkey. Brain Research. 1982; 234(2):435–441. [PubMed: 6800568]

Pikkarainen M, Pitkänen A. Projections from the lateral, basal and accessory basal nuclei of the amygdala to the perirhinal and postrhinal cortices in rat. Cerebral Cortex. 2001; 11(11):1064–1082. [PubMed: 11590116]

Pitkanen A, Kelly JL, Amaral DG. Projections from the lateral, basal, and accessory basal nuclei of the amygdala to the entorhinal cortex in the macaque monkey. Hippiocampus. 2002; 12(2):186–205.

Pitkänen A, Pikkarainen M, Nurminen N, Ylinen A. Reciprocal connections between the amygdala and the hippocampal formation, perirhinal cortex, and postrhinal cortex in rat. A review. Annals of the New York Academy of Sciences. 2000; 911:369–391. [PubMed: 10911886]

Posner MI, Petersen SE. The attention system of the human brain. Annual Review of Neuroscience. 1990; 13:25–42.

Ranganath C, Ritchey M. Two cortical systems for memory-guided behaviour. Nature Reviews Neuroscience. 2012; 13(10):713–26. [PubMed: 22992647]

Romanski LM, LeDoux JE. Equipotentiality of thalamo-amygdala and thalamo-cortico-amygdala circuits in auditory fear conditioning. The Journal of Neuroscience. 1992; 12(11):4501–9. [PubMed: 1331362]

Room P, Groenewegen HJ. Connections of the parahippocampal cortex. I. Cortical afferents. The Journal of Comparative Neurology. 1986; 251(4):415–450. [PubMed: 2431008]

Saksida LM, Bussey TJ, Buckmaster CA, Murray EA. Impairment and facilitation of transverse patterning after lesions of the perirhinal cortex and hippocampus, respectively. Cerebral Cortex. 2007; 17(1):108–15. [PubMed: 16452641]

Schmued LC, Fallon JH. Fluoro-Gold: a new fluorescent retrograde axonal tracer with numerous unique properties. Brain Research. 1986; 377(1):147–154. [PubMed: 2425899]

Shipp S. The brain circuitry of attention. Trends in Cognitive Sciences. 2004; 8(5):223–30. [PubMed: 15120681]

Sparta DR, Smithuis J, Stamatakis AM, Jennings JH, Kantak PA, Ung RL, Stuber GD. Inhibition of projections from the basolateral amygdala to the entorhinal cortex disrupts the acquisition of contextual fear. Frontiers in Behavioral Neuroscience. 2014; 8:129. [PubMed: 24834031]

Sugase-Miyamoto Y, Richmond BJ. Cue and reward signals carried by monkey entorhinal cortex neurons during reward schedules. Experimental Brain Research. 2007; 181(2):267–276. [PubMed: 17396249]

Suzuki WA, Amaral DG. Perirhinal and parahippocampal cortices of the macaque monkey: Cytoarchitectonic and chemoarchitectonic organization. The Journal of Comparative Neurology. 2003; 463(1):67–91. [PubMed: 12811804]

Swanson, LW. Brain Maps: Structure of the Rat Brain. Amsterdam: Elsevier; 1992.

Swanson, LW. Brain Maps: Structure of the Rat Brain. Amsterdam: Elsevier; 1998.

Unal G, Pare JF, Smith Y, Pare D. Differential connectivity of short- vs. long-range extrinsic and intrinsic cortical inputs to perirhinal neurons. The Journal of Comparative Neurology. 2013; 521(11):2538–50. [PubMed: 23296922]

Van der Werf YD, Witter MP, Groenewegen HJ. The intralaminar and midline nuclei of the thalamus. Anatomical and functional evidence for participation in processes of arousal and awareness. Brain Research. Brain Research Reviews. 2002; 39(2–3):107–40. [PubMed: 12423763]

van Groen T, Kadish I, Wyss JM. Efferent connections of the anteromedial nucleus of the thalamus of the rat. Brain Research. Brain Research Reviews. 1999; 30(1):1–26. [PubMed: 10407123]

Vertes RP, Crane AM, Colom LV, Bland BH. Ascending projections of the posterior nucleus of the hypothalamus: PHA-L analysis in the rat. The Journal of Comparative Neurology. 1995; 359(1): 90–116. [PubMed: 8557849]

Wan H, Aggleton JP, Brown MW. Different contributions of the hippocampus and perirhinal cortex to recognition memory. The Journal of Neuroscience. 1999; 19(3):1142–8. [PubMed: 9920675]

Winters BD, Bussey TJ. Transient inactivation of perirhinal cortex disrupts encoding, retrieval, and consolidation of object recognition memory. The Journal of Neuroscience. 2005; 25(1):52–61. [PubMed: 15634766]

Witter MP, Naber PA, van Haeften T, Machielsen WCM, Rombouts SARB, Barkhof F, Scheltens P, da Silva FHL. Cortico-hippocampal communication by way of parallel parahippocampal-subicular pathways. Hippocampus. 2000; 10(4):398–410. [PubMed: 10985279]

Witter MP, Room P, Groenewegen HJ, Lohman AH. Reciprocal connections of the insular and piriform claustrum with limbic cortex: an anatomical study in the cat. Neuroscience. 1988; 24(2):519–539. [PubMed: 3362351]

Wouterlood FG. Innervation of Entorhinal Principal Cells by Neurons of the Nucleus Reuniens Thalami. Anterograde PHA-L Tracing Combined with Retrograde Fluorescent Tracing and Intracellular Injection with Lucifer Yellow in the Rat. The European Journal of Neuroscience. 1991; 3(7):641–647. [PubMed: 12106472]

Zhu XO, Brown MW. Changes in neuronal activity related to the repetition and relative familiarity of visual stimuli in rhinal and adjacent cortex of the anaesthetised rat. Brain Research. 1995; 689(1): 101–10. [PubMed: 8528693]

Zola-Morgan S, Squire LR, Alvarez-Royo P, Clower RP. Independence of memory functions and emotional behavior: separate contributions of the hippocampal formation and the amygdala. Hippocampus. 1991; 1(2):207–20. [PubMed: 1669294]

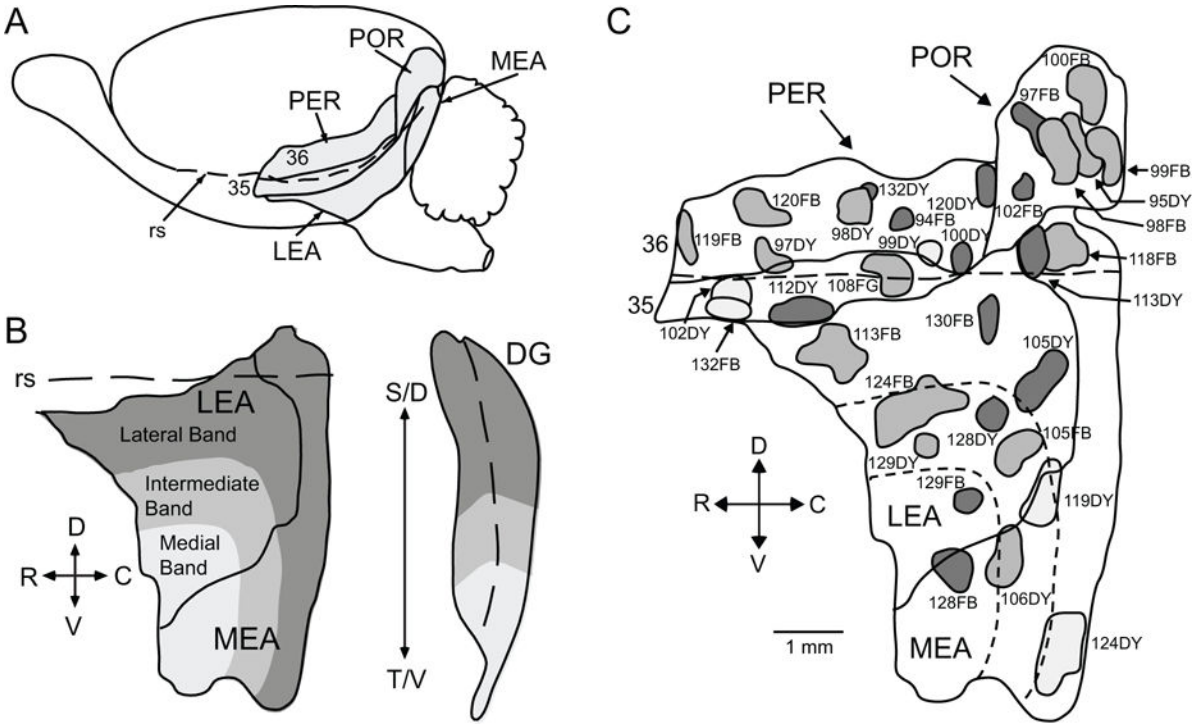

Figure 1.

PER, POR, and EC of the rat. A. Lateral surface view of the rat brain illustrating the borders. B. EC bands according to projections to the dentate gyrus (DG) of the hippocampus. The solid line delineates the border between LEA and MEA, the dashed line in the EC represents the rhinal sulcus and the dashed line in the DG represents the crest of the DG. The lateral band, represented in dark grey projects to the most septal (dorsal) region of the DG, the intermediate band, in medium grey, projects to intermediate DG, and the medial band, in light grey, projects to the most temporal (ventral) region of the DG. C. Location of labeled cells injection sites. The locations of the 33 injection sites are shown on a representative unfolded map of the PER (areas 35 and 36), POR and EC (LEA and MEA). Long dashed line represents the rhinal sulcus, small dashed lines represent the dentate-gyrus projecting bands for LEA and MEA. Sites shown in dark gray were restricted to deep layers. Sites shown in light gray were restricted to superficial layers. Sites shown in middle gray involved both deep and superficial layers. Other abbreviations: C, caudal; D, dorsal; R, rostral; rs, rhinal sulcus; S, septal; T, temporal; V, ventral. Scale bar: 1 mm.

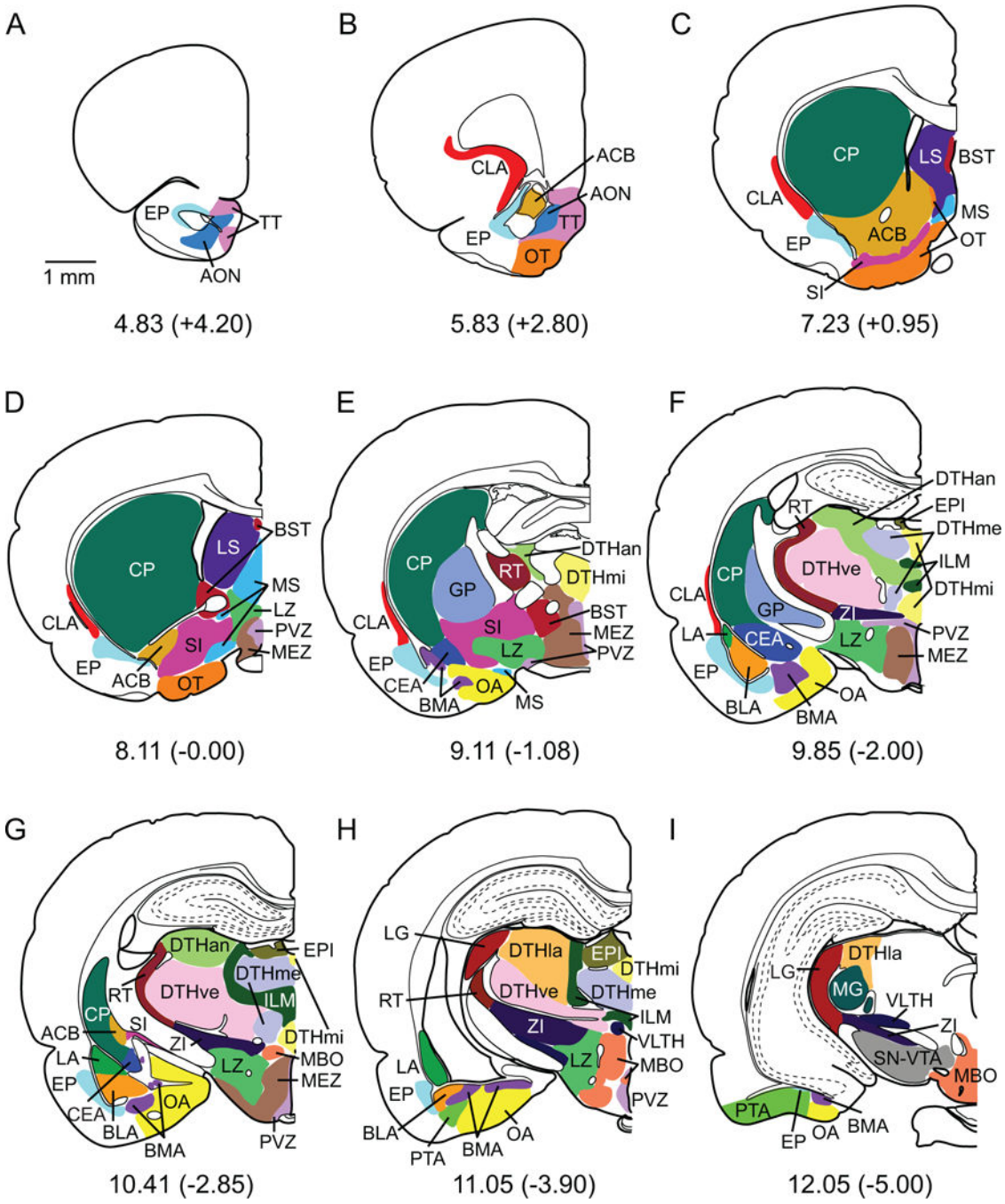

Figure 2.

Boundaries for subcortical nuclei for a subset of coronal sections. The boundaries and coronal views were adapted from Swanson (1998). Some nuclei were combined as described in the Nomenclature section. Each structure is depicted in a unique color. See list of abbreviations in Table 1. Scale bar: 1 mm.

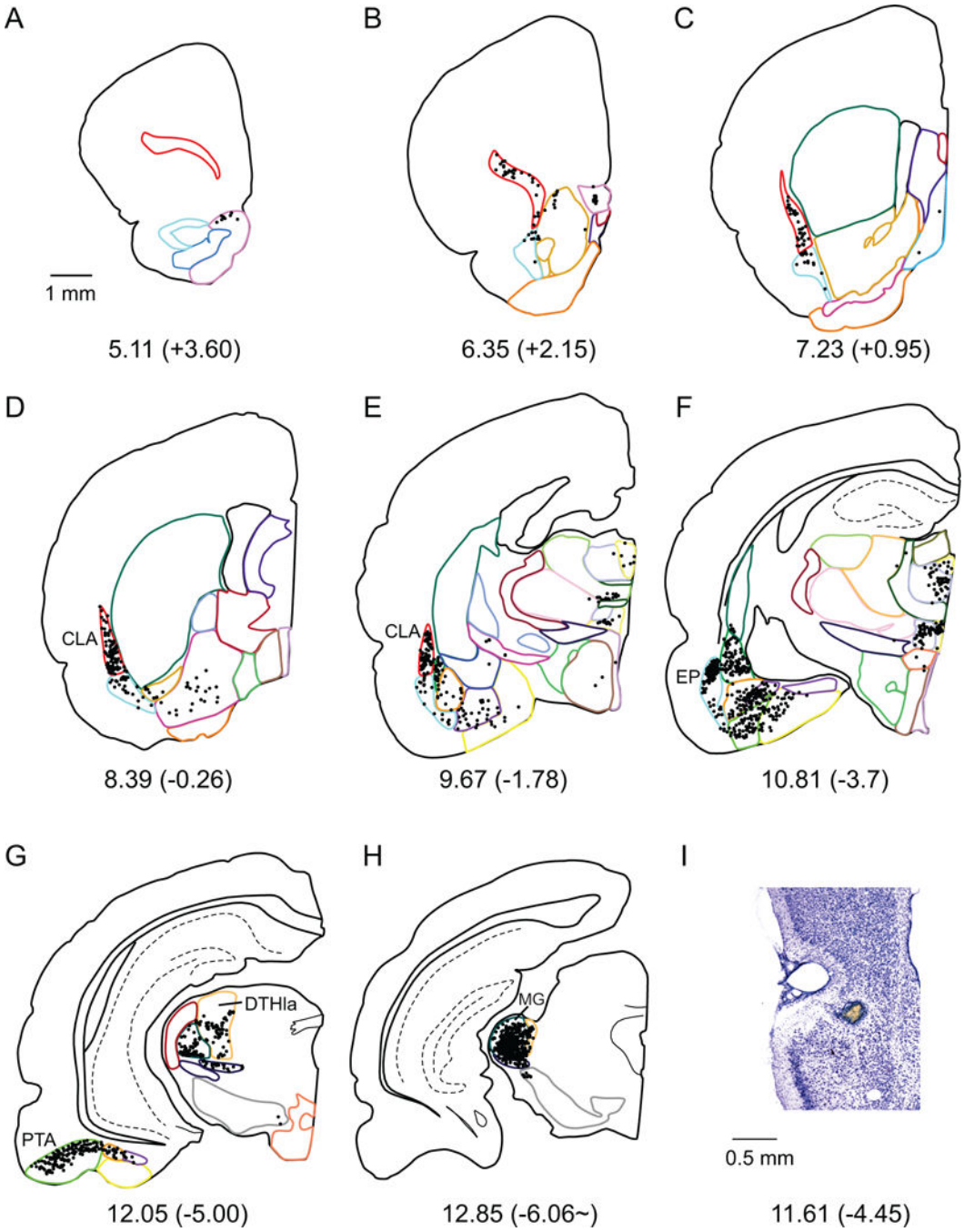

Figure 3.

A–H. Computer generated plots of coronal sections showing the distribution of labeled cells arising from a labeled cells tracer injection in Area 35. Eight of 44 rostrocaudal levels are shown for experiment 112DY. Boundaries of subcortical structures are depicted by colored contours. See Figure 2 for color code. Note the high density of cells observed in CLA, EP, PTA and MG. MG labeling was denser in this case than all the other PER area 35 injection cases. I. Injection site on a Nissl stained section. The injection site is not represented in the diagram, because it was located between panels F and G.

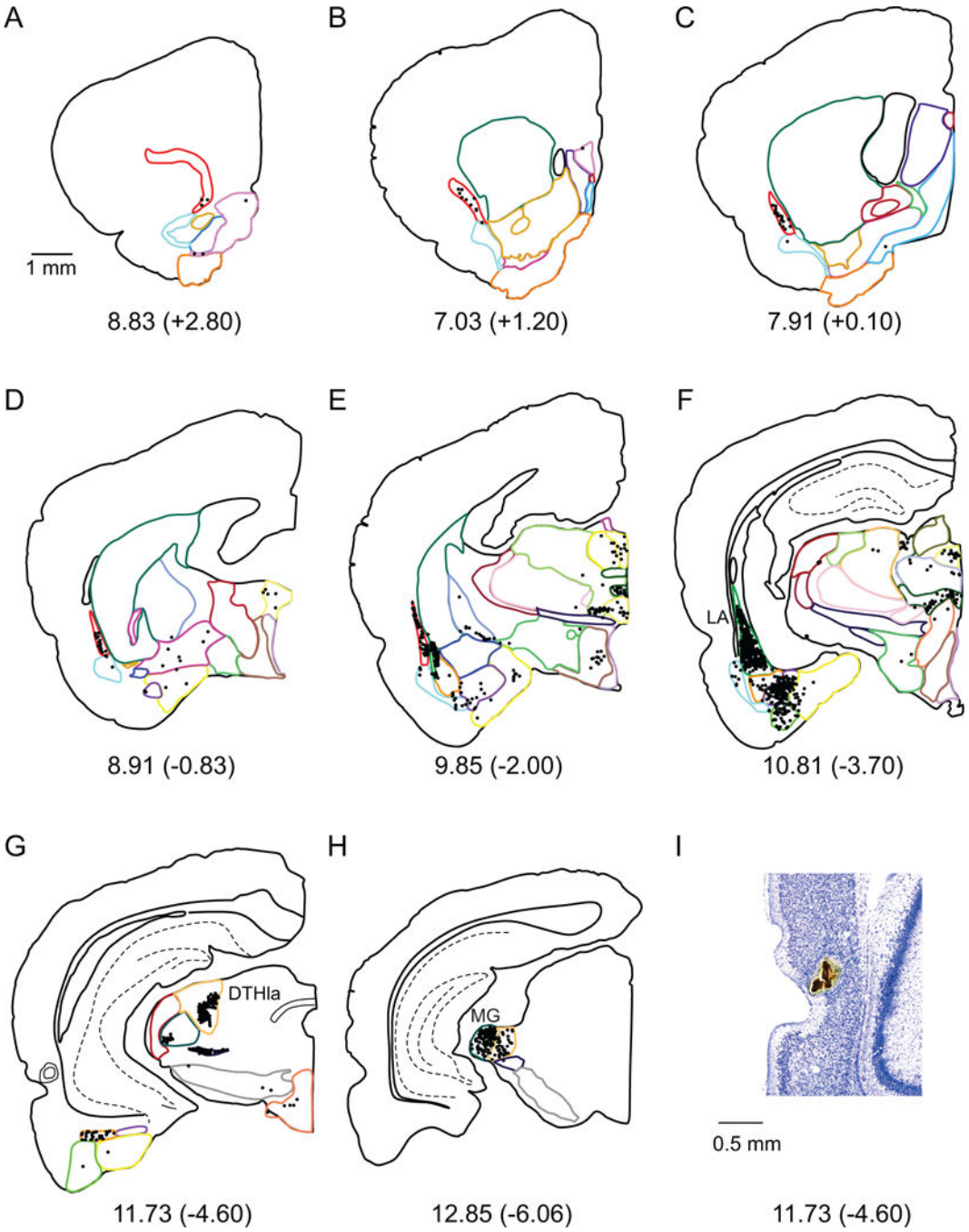

Figure 4.

A–H. Computer generated plots of coronal sections showing the distribution of labeled cells arising from a labeled cells tracer injection in Area 36 (concentric circles marked in panel G) and. Eight of 43 coronal levels are shown for experiment 98DY. Boundaries of subcortical structures are depicted by colored contours. See Figure 2 for color code. Note high density of cells in LA, DTHla (specifically the supragenicular nucleus) and MG. I. Injection site on a Nissl stained section.

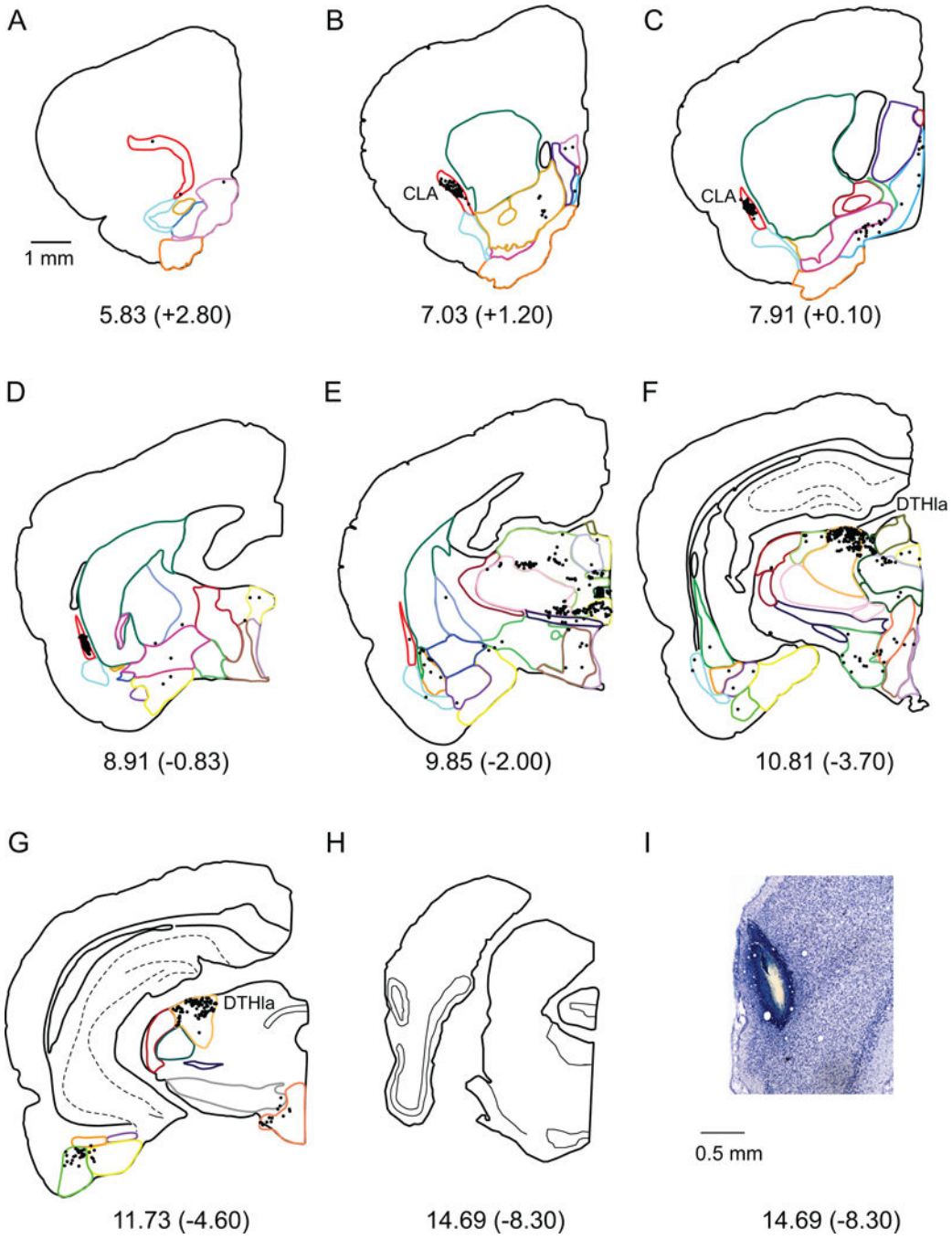

Figure 5.

A–H. Computer generated plots of coronal sections showing the distribution of labeled cells arising from a connectional topography tracer injection in the POR (shown in panel H). Eight of 43 rostrocaudal levels are shown for experiment 98FB. Boundaries of subcortical structures are depicted by colored contours. See Figure 2 for color code. Note the overall lower number of labeled cells, but the high density of cells in CLA and DTHla (specifically, the lateral posterior nucleus). I. Injection site on a Nissl stained section.

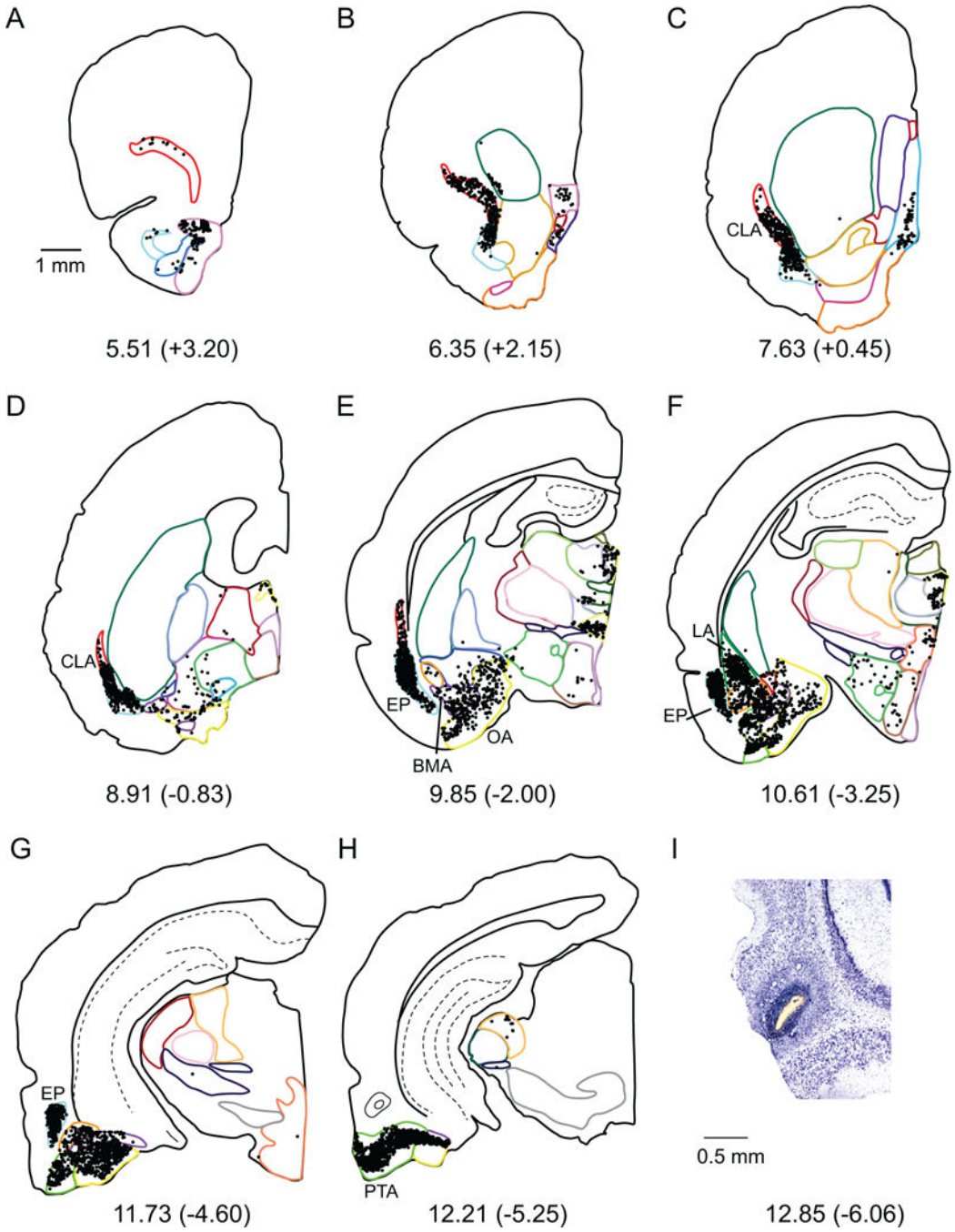

Figure 6.

A–H. Computer generated plots of coronal sections showing the distribution of labeled cells arising from a retrograde tracer injection in the LEA (shown in panel H). Eight of 48 rostrocaudal levels are shown for experiment 124FB. Boundaries of subcortical structures are depicted by colored contours. See Figure 2 for color code. Note the high density of cells in CLA, EP, LA, BMA, OA, and PTA. I. Injection site on a Nissl stained section.

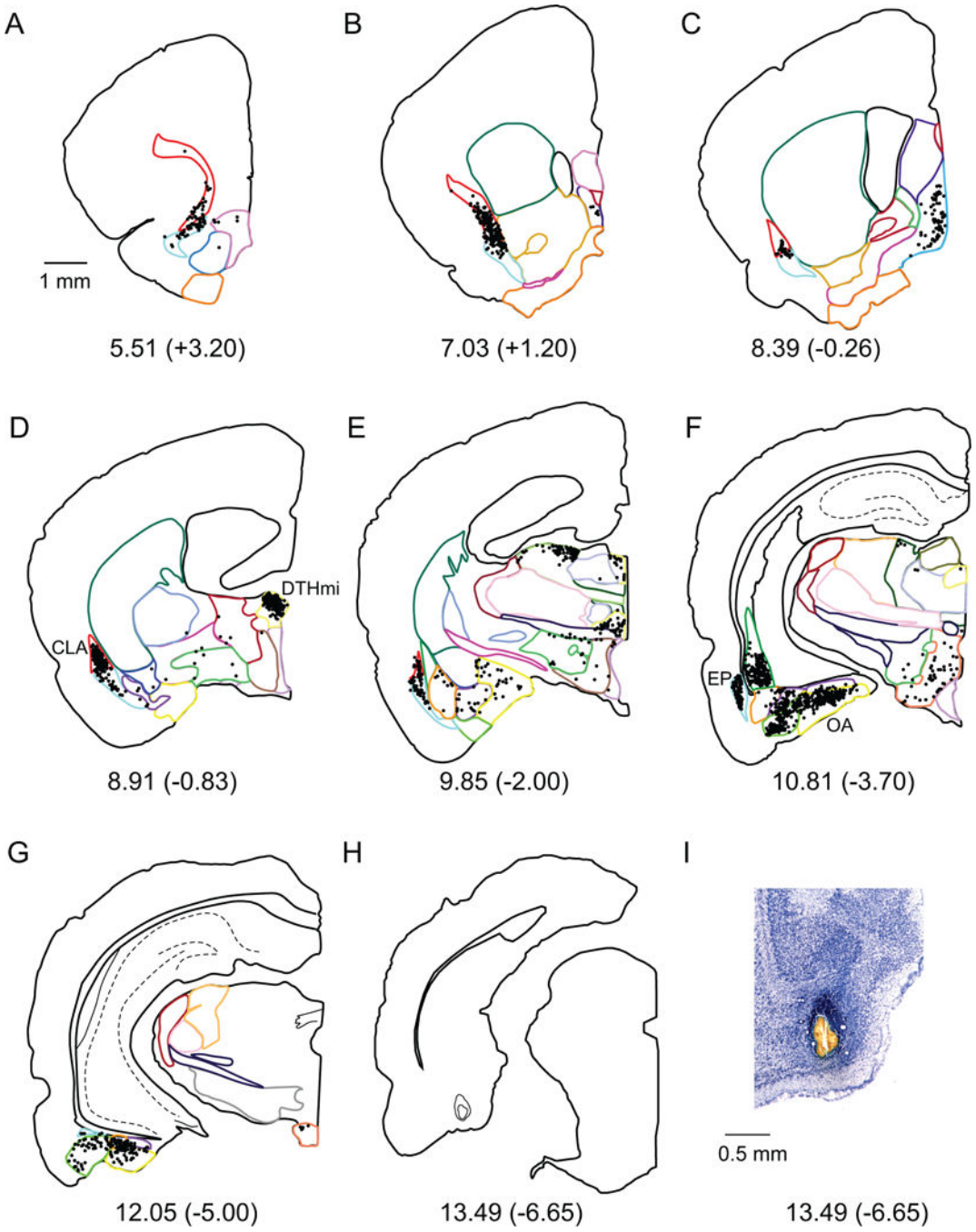

Figure 7.

A–H. Computer generated plots of coronal sections showing the distribution of labeled cells arising from a retrograde tracer injection in the MEA (shown in panel H). Eight of 44 rostrocaudal levels are shown for experiment 106DY. Boundaries of subcortical structures are depicted by colored contours. See Figure 2 for color code. Note the high density of labeled cells in CLA, DTHmi (specifically the nucleus reuniens), EP and OA. I. Injection site on a Nissl stained section.

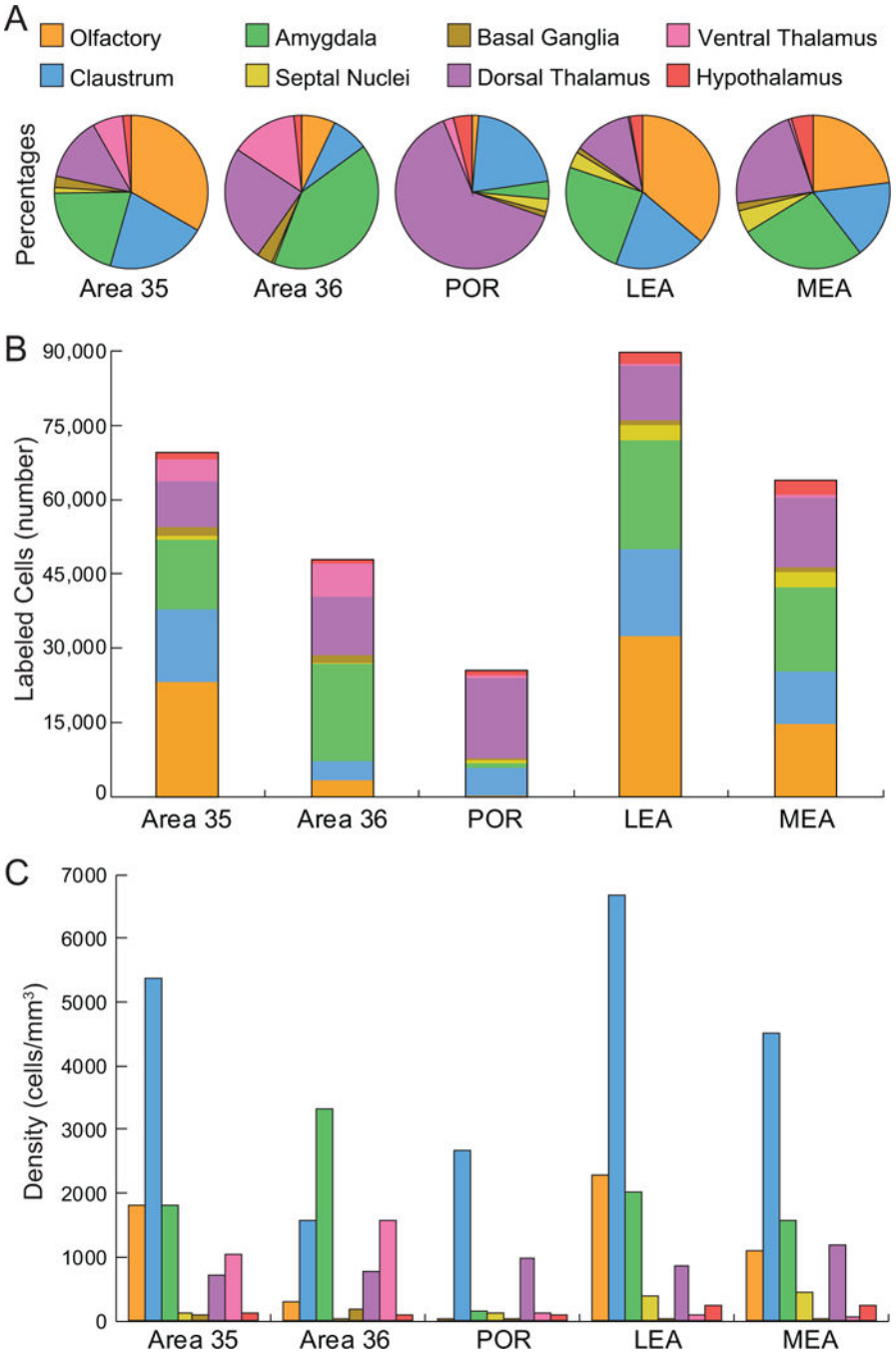

Figure 8.

Percentages, total numbers of labeled cells and densities in composite subcortical areas resulting from retrograde injections in the PER areas 35 and 36, POR, LEA and MEA. Color code is for all panels. A. Input to each target region as indicated by the percentage of labeled cells found in each composite subcortical region. Note POR has a much larger proportion of labeled cells in the dorsal thalamic nuclei, largely the lateral posterior nucleus. Proportions for area 35 are more similar to the LEA and area 36 is more similar to the MEA. See Table 3 for details. B. Input to each target region as indicated by normalized total numbers of labeled

cells for each group of subcortical structures. The LEA has the most input from subcortical regions, followed by area 35, then MEA, area 36 and finally the POR. C. Output from different subcortical structures indicated by average densities of labeled cells in the subcortical areas. See Table 4 for details and Table 1 for abbreviations.

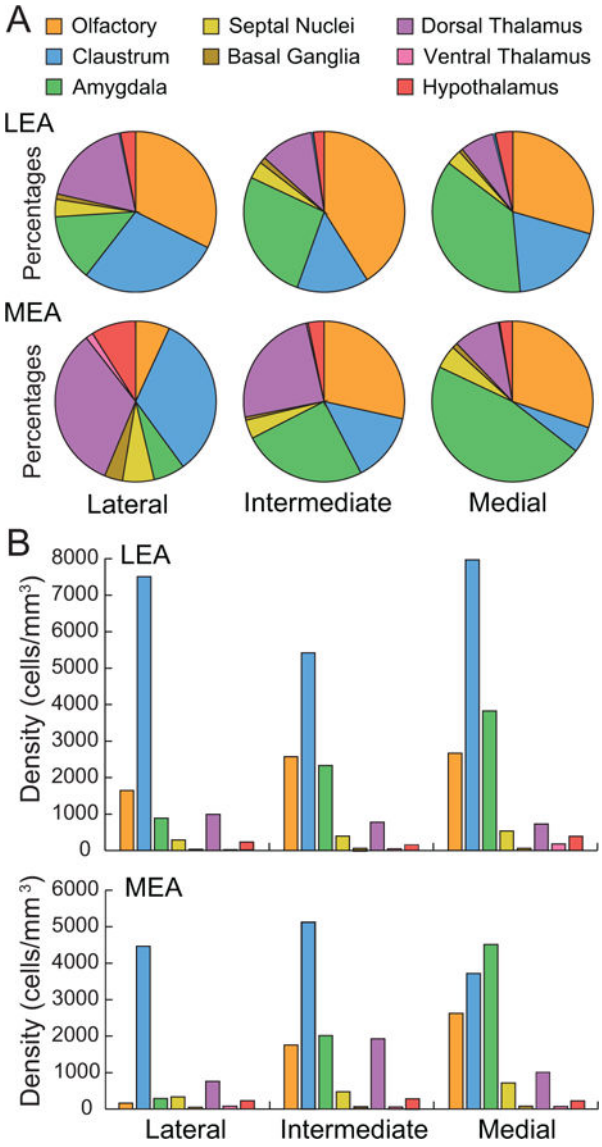

Figure 9.

Percentages and densities and labeled cells in the lateral, intermediate, and medial DG-projecting bands of the LEA and the MEA. A. Input to each LEA and MEA band as indicated by percentage of labeled cells found in each composite subcortical region. Color code in panel A also serves for panel B. The distribution of subcortical input is generally similar between the LEA and MEA bands. Amygdala input increases from the lateral to the medial bands of both LEA and MEA. Olfactory input increases from the lateral to the medial bands of MEA. Input from the claustrum decreases from lateral to medial bands for the MEA. B. Output to different bands indicated by densities of labeled cells. Average densities of labeled cells in the subcortical areas. Olfactory and amygdala structures target the medial band of both the LEA and the MEA more strongly than the lateral and intermediate bands.

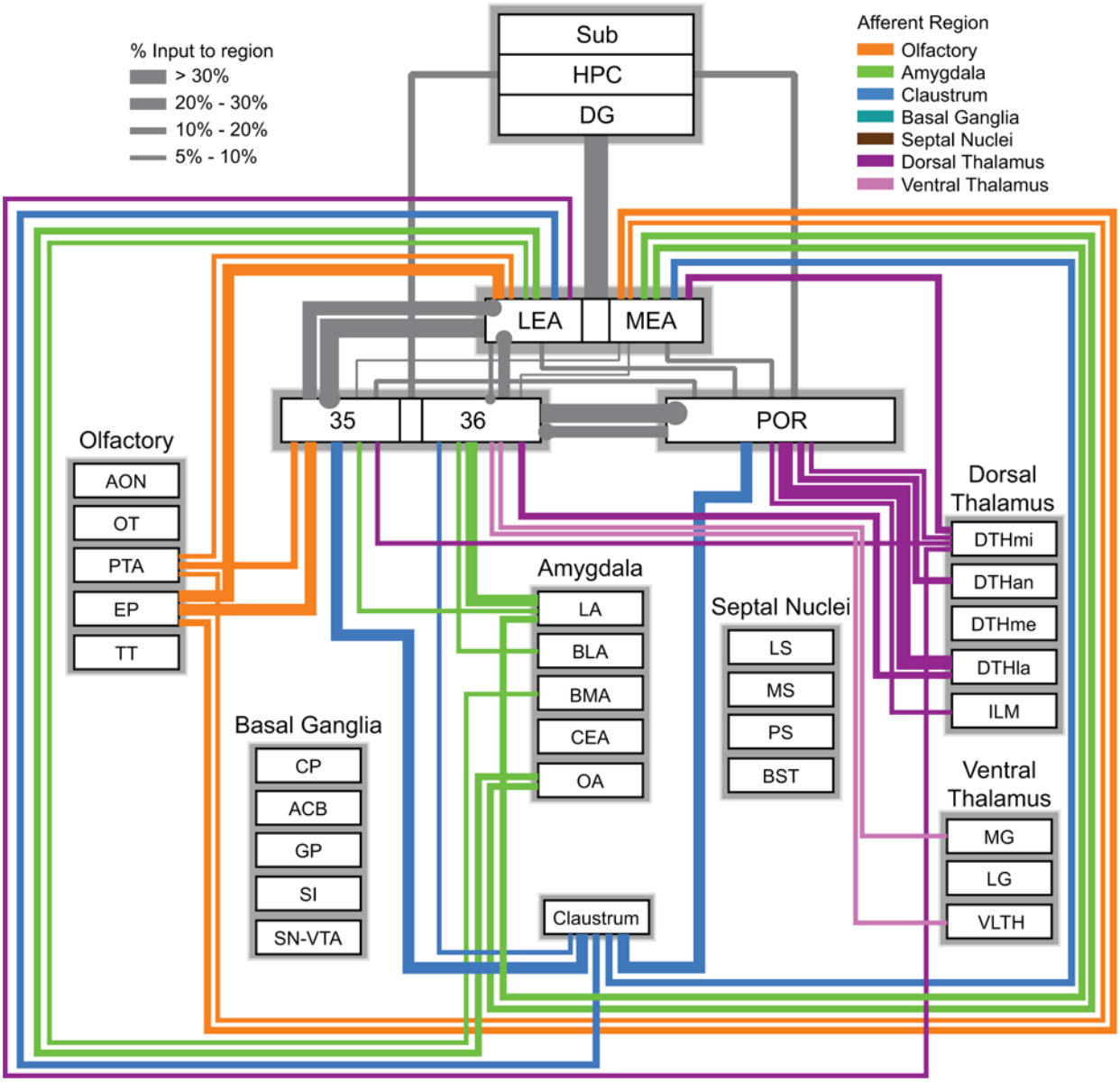

Figure 10.

Wiring diagram based on the percentage measure representing the subcortical input to the PER areas 35 and 36, POR, LEA and MEA. Colors represent the afferent regions. Thickness of the bars represents the percentage of input to each target region. This measure is useful for comparing the pattern of inputs at the target regions. For example, PER area 35 receives a strong input from olfactory structures, whereas area 36 does not. Information for connections shown in grey are from prior studies (Agster and Burwell, 2013; Burwell and Amaral, 1998b). For simplicity, the weakest connections (<5%) are not shown but can be found in Table 3. All basal ganglia connections were below 5%. See Table 1 for a list of abbreviations.

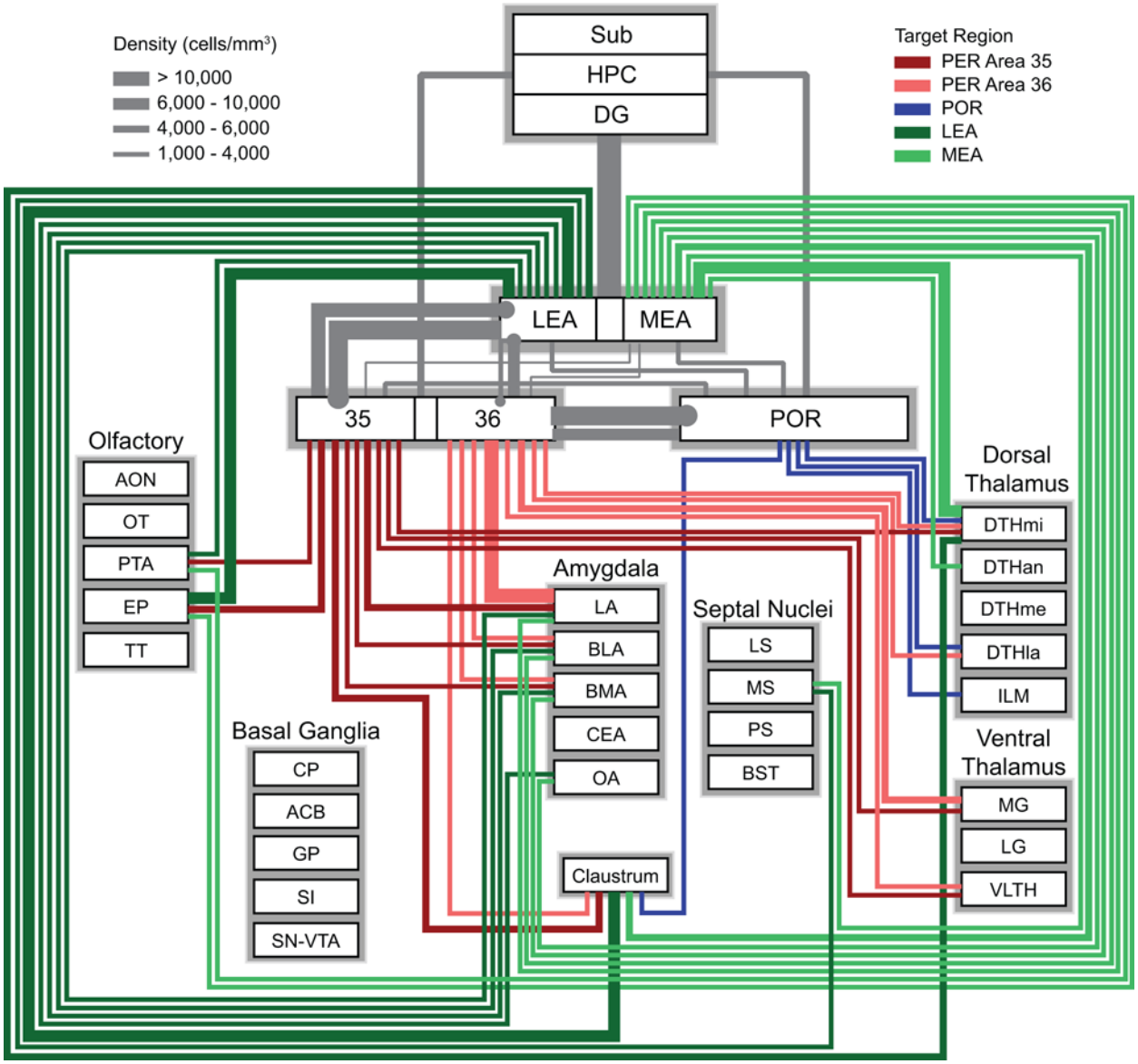

Figure 11.

Wiring diagram based on the density measure representing subcortical output to PER areas 35 and 36, POR, LEA, and MEA). Colors represent the different target regions. Thickness of the bars represents the density of labeling in the afferent regions. This measure is useful for comparing the pattern of output of particular subcortical afferent structures to different targets. For example, the claustrum provides output to all five structures, but the strengths of those projections differ. Information for connections shown in grey are from prior studies (Agster and Burwell, 2013; Burwell and Amaral, 1998b). For simplicity, the weakest connections (< 2000 labeled cells/mm^3) are not shown but can be found in Table 4. All basal ganglia connections were below 2000 cells/mm^3. See Table 1 for a list of abbreviations.

Table 1

Nomenclature and Abbreviations

Regions Analyzed	Abbreviation
Olfactory Regions	
Anterior Olfactory Nucleus	AON
Olfactory Tubercle	OT
Piriform Transition Area	PTA
Endopiriform	EP
Taenia Tecta	TT
Claustrum	CLA
Amygdala	
Lateral Nucleus	LA
Basolateral Nucleus	BLA
Basomedial Nucleus	BMA
Central Nucleus	CEA
Olfactory Amygdala	OA
Septal Nuclei	
Lateral Septum	LS
Medial Septum	MS
Posterior Septum	PS
Bed Nucleus of the Stria Terminalis	BST
Basal Ganglia	
Caudate Putamen	CP
Nucleus Accumbens	ACB
Globus Pallidus	GP
Substantia Innominata	SI
Substantia Nigra-Ventral Tegmental Area	SN-VTA
Dorsal Thalamus	
Epithalamus	EPI
Dorsal Midline Group	DTHmi
Dorsal Anterior Group	DTHan
Dorsal Medial Group	DTHme
Dorsal Lateral Group	DTHla
Dorsal Ventral Group	DTHve
Intralaminar Nuclei	ILM
Ventrolateral Thalamus	
Medial Geniculate	MG
Lateral Geniculate	LG
Reticular Nucleus	RT
Zona Incerta	ZI
Ventrolateral Group	VLTH
Hypothalamus	

Regions Analyzed	Abbreviation
Periventricular Zone	PVZ
Medial Zone	MEZ
Mammillary Bodies	MBO
Lateral Zone	LZ

Nomenclature is from Paxinos and Watson (1998) and Swanson (1998). DTHmi included the paraventricular nucleus, the parataenial nucleus, and the nucleus reuniens; DTHan included anteroventral, anteromedial, anterodorsal, interanteromedial, interanterodorsal, and lateral dorsal nuclei; DTHme included mediodorsal and submedial thalamic nuclei, and the perireuniens nucleus; DTHla included the suprageniculate nucleus and the lateral posterior nucleus, the posterior limiting nucleus, and the posterior complex of the thalamus; DTHve included the ventral anterior-lateral complex, the ventral medial nucleus and the ventral posterior complex of the dorsal thalamus; VLTH included the subthalamic nucleus, the perifascicular nucleus, and the peripeduncular nucleus; PVZ included the paraventricular, anteroventral, anterior, intermediate, and posterior paraventricular hypothalamic nuclei; MBO included the dorsal, medial, and lateral mammillary nuclei, the tuberomammillary nucleus, and the supramammillary nucleus; MEZ included the medial, anterodorsal, anteroventral, and posterodorsal preoptic nuclei, the parastrial nucleus, the suprachismatic nucleus, the retrochiasmatic area, the subparaventriclar zone, the anterior hypothalamic area, and the tuberal area of the hypothalamus. The LZ included the lateral preoptic area and the lateral hypothalamic area. See text for details.

Table 2

Labeled cells Tracer Injection Sites

Location of Injection	Experiment	Layer	Size (mm^3)
Perirhinal Cortex (PER)			
rostral area 35	102DY	I–III	0.06
rostroventral area 35	132FB[1]	I–II	0.02
ventral area 35	112DY	V	0.10
caudal area 35	108FG	I–VI	0.24
rostral area 36	119FB	I–V	0.08
rostrodorsal area 36	120FB	III–V	0.11
rostroventral area 36	97DY	III–V	0.06
mid-rostrocaudal area 36	98DY	I–V	0.11
mid-rostrocaudal area 36	132DY	V	0.02
mid-rostrocaudal area 36	94FB	V	0.02
caudoventral area 36	99DY	II–III	0.06
caudoventral area 36	100DY	V	0.01
caudodorsal area 36	120DY	V	0.02
Postrhinal Cortex (POR)			
rostroventral POR	102FB	V	0.02
rostral POR	97FB	V	0.16
middle POR	98FB	I–VI	0.13
middle POR	95DY	III–VI	0.13
caudodorsal POR	100FB	I–V	0.17
caudal POR	99FB	I–V	0.13
Entorhinal Cortex (EC)			
rostrolateral LEA, LB	113FB	I–V	0.19
caudolateral LEA, LB	130FB	V–VI	0.04
caudal LEA, LB	105DY	V	0.06
rostral LEA, IB	124FB	I–VI	0.32
rostral LEA, IB	129DY	III–V	0.05
middle LEA, IB	128DY	V	0.04
caudomedial LEA, IB	105FB[2]	III–VI	0.02
caudomedial LEA, MB	129FB	V–VI	0.02
dorsolateral MEA, LB	113DY	V	0.05
dorsolateral MEA, LB	118FB	III–VI	0.13
mediolateral MEA, LB	124DY	I–III	0.18
caudoventral MEA, IB	119DY	I–II	0.07
ventral MEA, IB	106DY	II–VI	0.10
rostroventral MEA, MB	128FB	V	0.06

Table is adapted from Burwell and Amaral (1998a). The regional and laminar location of the injection sites are shown in the first and third columns. Labeled cells tracers were Diamidino Yellow (DY), Fast Blue (FB), and Fluoro-Gold (FG). Each experiment is designated as the subject identifier followed by the tracer.

[1]For experiment 132FB, moderate necrosis was observed in the external capsule.

[2]Experiment 105FB slightly involved underlying white matter.

Table 3

Percentages of Total Input to Target Regions

Afferent Regions	Target Regions				
	Area 35	Area 36	POR	LEA	MEA
Olfactory	**33.3**	**7.1**	**1.4**	**36.2**	**23.0**
AON	0.9 ± 0.3	0.1 ± 0.1	0.0 ± 0.0	0.4 ± 0.1	0.3 ± 0.2
OT	0.1 ± 0.0	0.1 ± 0.0	0.0 ± 0.0	0.1 ± 0.0	0.1 ± 0.0
PTA	10.6 ± 0.8	4.5 ± 1.6	0.9 ± 0.4	9.3 ± 2.2	5.3 ± 2.4
EP	20.4 ± 2.5	2.0 ± 0.7	0.3 ± 0.1	24.9 ± 3.5	16.3 ± 7.2
TT	1.3 ± 0.3	0.4 ± 0.3	0.1 ± 0.0	1.5 ± 0.3	1.0 ± 0.5
Claustrum	**21.1 ± 4.5**	**7.8 ± 2.1**	**21.4 ± 3.0**	**19.5 ± 3.5**	**16.5 ± 5.0**
Amygdala	**20.4**	**40.9**	**3.8**	**24.6**	**26.7**
LA	7.0 ± 1.6	28.9 ± 8.1	1.5 ± 0.5	4.9 ± 1.1	5.9 ± 3.1
BLA	3.5 ± 1.2	5.8 ± 1.8	1.1 ± 0.3	2.6 ± 0.7	2.2 ± 0.9
BMA	4.8 ± 0.7	4.6 ± 1.3	0.6 ± 0.2	6.1 ± 1.7	4.7 ± 3.0
CEA	0.2 ± 0.1	0.1 ± 0.0	0.0 ± 0.0	0.2 ± 0.1	0.0 ± 0.0
OA	4.9 ± 0.4	1.6 ± 0.4	0.5 ± 0.3	10.8 ± 3.2	13.9 ± 8.4
Septal Nuclei	**1.2**	**0.5**	**2.7**	**3.4**	**4.8**
LS	0.2 ± 0.1	0.0 ± 0.0	0.0 ± 0.0	0.2 ± 0.0	0.3 ± 0.1
MS	1.0 ± 0.5	0.4 ± 0.2	2.6 ± 0.5	3.1 ± 0.8	4.3 ± 0.8
PS	0.0 ± 0.0	0.0 ± 0.0	0.0 ± 0.0	0.1 ± 0.0	0.1 ± 0.0
BST	0.0 ± 0.0	0.0 ± 0.0	0.0 ± 0.0	0.1 ± 0.0	0.2 ± 0.1
Basal Ganglia	**2.4**	**3.3**	**1.2**	**1.1**	**1.6**
CP	0.2 ± 0.0	1.2 ± 0.8	0.3 ± 0.1	0.2 ± 0.1	0.5 ± 0.2
ACB	0.3 ± 0.1	0.1 ± 0.1	0.1 ± 0.0	0.1 ± 0.0	0.1 ± 0.0
GP	0.1 ± 0.0	0.2 ± 0.1	0.1 ± 0.0	0.0 ± 0.0	0.1 ± 0.0
SI	1.7 ± 0.2	1.2 ± 0.1	0.4 ± 0.1	0.7 ± 0.2	0.6 ± 0.1
SN-VTA	0.2 ± 0.1	0.7 ± 0.5	0.3 ± 0.1	0.1 ± 0.0	0.4 ± 0.1
D. Thalamus	**13.5**	**24.6**	**63.6**	**12.2**	**22.1**
EPI	0.0 ± 0.0	0.9 ± 0.9	0.1 ± 0.1	0.0 ± 0.0	0.0 ± 0.0
DTHmi	5.6 ± 1.0	3.9 ± 0.8	6.7 ± 0.9	8.7 ± 2.6	13.0 ± 3.6

Afferent Regions	Target Regions				
	Area 35	**Area 36**	**POR**	**LEA**	**MEA**
DTHan	0.3 ± 0.2	0.4 ± 0.2	10.3 ± 2.3	1.4 ± 0.8	4.7 ± 1.1
DTHme	1.2 ± 0.1	0.8 ± 0.3	1.2 ± 0.2	0.6 ± 0.1	0.3 ± 0.1
DTHla	4.2 ± 0.9	15.6 ± 3.0	34.5 ± 5.3	0.4 ± 0.2	2.2 ± 1.2
DTHve	0.4 ± 0.2	1.0 ± 0.5	2.1 ± 0.5	0.1 ± 0.0	0.3 ± 0.2
ILM	1.7 ± 0.2	1.8 ± 0.5	8.8 ± 1.3	0.9 ± 0.3	1.6 ± 0.4
V.L. Thalamus	**6.4**	**14.1**	**2.2**	**0.4**	**0.7**
MG	4.5 ± 4.1	8.7 ± 2.7	0.1 ± 0.0	0.0 ± 0.0	0.1 ± 0.1
LG	0.0 ± 0.0	0.0 ± 0.0	0.3 ± 0.2	0.0 ± 0.0	0.0 ± 0.0
RT	0.0 ± 0.0	0.0 ± 0.0	0.1 ± 0.0	0.0 ± 0.0	0.0 ± 0.0
ZI	0.2 ± 0.0	0.3 ± 0.1	0.9 ± 0.1	0.1 ± 0.0	0.4 ± 0.1
VLTH	1.6 ± 0.3	5.1 ± 1.2	0.7 ± 0.1	0.2 ± 0.1	0.1 ± 0.0
Hypothalamus	**1.8**	**1.6**	**4.0**	**2.7**	**4.6**
PVZ	0.0 ± 0.0	0.1 ± 0.0	0.1 ± 0.0	0.1 ± 0.0	0.1 ± 0.0
MEZ	0.3 ± 0.2	0.3 ± 0.1	0.5 ± 0.2	0.3 ± 0.1	0.4 ± 0.2
MBO	0.6 ± 0.3	0.6 ± 0.2	1.5 ± 0.4	1.3 ± 0.4	2.1 ± 0.5
LZ	0.8 ± 0.3	0.6 ± 0.1	1.9 ± 0.4	1.0 ± 0.2	2.0 ± 0.8
Total Percent	**100**	**100**	**100**	**100**	**100**
Total SC Cells	**69,400**	**47,900**	**25,500**	**89,800**	**63,800**

Percent ± SEM of total labeled cells observed in each subcortical region for each target region. The normalized mean total labeled subcortical cells for each region is rounded to the nearest 100. Labeled cells in a subcortical region can be calculated by taking the percentage of the total labeled cells.

Table 4

Density of Labeled cells in Afferent Regions

Afferent Regions	Target Regions				
	Area 35	**Area 36**	**POR**	**LEA**	**MEA**
Olfactory	**1803**	**297**	**36**	**2275**	**1102**
AON	540 ± 220	58 ± 42	1 ± 1	171 ± 50	78 ± 50
OT	20 ± 9	17 ± 13	2 ± 1	12 ± 3	16 ± 8
PTA	3652 ± 655	988 ± 331	125 ± 67	3992 ± 597	1657 ± 802
EP	4325 ± 560	314 ± 95	32 ± 9	6562 ± 887	3439 ± 1578
TT	478 ± 94	110 ± 76	19 ± 7	640 ± 115	321 ± 153
Claustrum	**5366 ± 847**	**1570 ± 423**	**2682 ± 395**	**6678 ± 1120**	**4509 ± 1417**
Amygdala	**1802**	**3325**	**150**	**2012**	**1565**
LA	4288 ± 1167	13181 ± 3803	403 ± 126	3840 ± 838	3363 ± 1812
BLA	2030 ± 833	2018 ± 550	228 ± 71	1853 ± 514	1037 ± 444
BMA	1922 ± 445	1242 ± 325	85 ± 31	2603 ± 674	1900 ± 1221
CEA	104 ± 43	27 ± 6	6 ± 5	165 ± 54	20 ± 7
OA	666 ± 97	155 ± 42	29 ± 19	1598 ± 440	1507 ± 853
Septal Nuclei	**118**	**43**	**106**	**399**	**443**
LS	48 ± 29	4 ± 3	4 ± 2	53 ± 9	61 ± 22
MS	407 ± 212	156 ± 85	417 ± 84	1430 ± 344	1608 ± 329
PS	0 ± 0	9 ± 5	3 ± 3	74 ± 40	45 ± 26
BST	15 ± 6	2 ± 2	1 ± 1	37 ± 13	56 ± 24
Basal Ganglia	**77**	**176**	**16**	**39**	**39**
CP	5 ± 1	397 ± 390	3 ± 1	8 ± 3	13 ± 6
ACB	29 ± 6	11 ± 5	4 ± 2	11 ± 3	7 ± 2
GP	14 ± 5	75 ± 59	13 ± 4	12 ± 3	16 ± 8
SI	285 ± 54	130 ± 8	30 ± 4	149 ± 40	92 ± 13
SN-VTA	51 ± 16	265 ± 234	29 ± 12	17 ± 4	68 ± 25
D. Thalamus	**714**	**763**	**981**	**873**	**1178**
EPI	15 ± 13	463 ± 428	45 ± 41	21 ± 11	24±22
DTHmi	2782 ± 614	1426 ± 323	1386 ± 170	4710 ± 1328	6021 ± 2022

Afferent Regions	Target Regions				
	Area 35	**Area 36**	**POR**	**LEA**	**MEA**
DTHan	86 ± 55	80 ± 32	946 ± 188	445 ± 233	1159 ± 344
DTHme	512 ± 69	250 ± 88	197 ± 33	317 ± 72	120 ± 52
DTHla	905 ± 190	2223 ± 369	2782 ± 412	107 ± 53	355 ± 164
DTHve	56 ± 24	272 ± 215	113 ± 25	10 ± 3	33 ± 21
ILM	640 ± 95	630 ± 253	1398 ± 293	499 ± 193	533 ± 137
V.L. Thalamus	**1029**	**1585**	**120**	**77**	**57**
MG	3206 ± 2903	4211 ± 1228	30 ± 9	30 ± 20	63 ± 41
LG	12 ± 10	14 ± 7	76 ± 48	11 ± 7	16 ± 10
RT	3 ± 2	5 ± 5	10 ± 4	5 ± 2	13 ± 8
ZI	72 ± 18	62 ± 18	105 ± 14	47 ± 10	99 ± 30
VLTH	1851 ± 304	3633 ± 830	377 ± 76	294 ± 115	92 ± 45
Hypothalamus	**113**	**80**	**90**	**242**	**235**
PVZ	30 ± 9	30 ± 12	14 ± 9	80 ± 42	41 ± 8
MEZ	76 ± 43	62 ± 14	43 ± 16	80 ± 29	88 ± 35
MBO	226 ± 121	143 ± 36	189 ± 38	605 ± 203	541 ± 151
LZ	121 ± 48	84 ± 24	114 ± 22	202 ± 45	271 ± 99

Density ± standard error of the mean (SEM) of labeled cells in each subcortical region (cells/mm^3). Density of labeled cells represents the number of cells in each region divided by its volume. Numbers in bold are averages for the collection of regions.